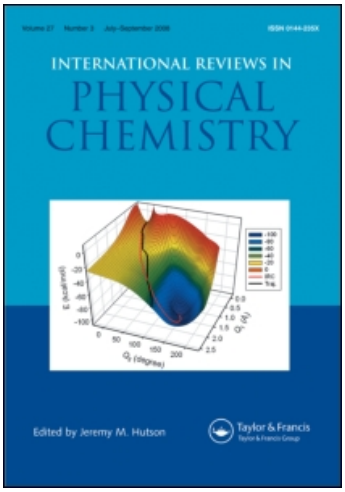

International Reviews in Physical Chemistry
Publication details, including instructions for authors and subscription information:
http://www.informaworld.com/smpp/title~content=t713724383

Statistical quantum studies on insertion atom-diatom reactions

Tomás González-Lezana[a]
[a] Instituto de Matemáticas y Física Fundamental (CSIC), Serrano 123, 28006 Madrid, Spain

To cite this Article González-Lezana, Tomás(2007) 'Statistical quantum studies on insertion atom-diatom reactions', International Reviews in Physical Chemistry, 26: 1, 29 — 91
To link to this Article: DOI: 10.1080/03081070600933476
URL: http://dx.doi.org/10.1080/03081070600933476

International Reviews in Physical Chemistry,
Vol. 26, No. 1, January–March 2007, 29–91

Taylor & Francis
Taylor & Francis Group

Statistical quantum studies on insertion atom–diatom reactions

TOMÁS GONZÁLEZ-LEZANA*

Instituto de Matemáticas y Física Fundamental (CSIC), Serrano 123,
28006 Madrid, Spain

(*Received 10 July 2006; in final form 24 July 2006*)

The study of insertion atom–diatom reactions is usually complicated by the existence of deep potential wells between reactants and products. The large number of bound and resonance states to be properly described makes exact quantum mechanical calculations extremely demanding in terms of numerical effort. In this type of collision, the process proceeds via the formation of an intermediate complex of finite lifetime. The application of statistical quantum methods provides a valid alternative to investigate the dynamics of the reaction. In this work, studies performed with a statistical quantum method recently developed by Rackham *et al*. on a variety of different reactions are extensively reviewed. The overall dynamics of the processes selected to test this statistical model range from complex-forming mechanisms to a competition between insertion and direct abstraction reaction pathways. This review includes studies of $X + H_2$ reactions, where X is one of the following electronically excited non-metallic atoms: $C(^1D)$, $N(^2D)$, $O(^1D)$ or $S(^1D)$. An ion–diatom collision, the H_3^+ system (with its isotope variants), is also investigated. Finally, results of the statistical study of the $H + O_2$ reaction are discussed. In all cases, comparison with both exact quantum mechanical calculations and experimental measurements shows that the method provides valid and rigorous information about the underlying dynamics of the reactions under study.

Contents

*Email: tglezana@imaff.cfmac.csic.es

International Reviews in Physical Chemistry
ISSN 0144–235X print/ISSN 1366–591X online
http://www.tandf.co.uk/journals
DOI: 10.1080/03081070600933476

1. Introduction

One of the most interesting features in the study of gas phase reactive atom–diatom collisions is the understanding of the intimate mechanisms which govern the reaction. In fact, in some cases, rather than a simple investigation of the kinetics of the process, the really challenging aspect to study is to know the steps which lead from reactants to products. In this sense, nowadays experimental techniques are almost capable of providing a step-by-step description of the collisions of gas molecules. Thus, by means of ultrashort pulse lasers it has been possible to characterize molecular processes which take place in the femtosecond regime [1–4]. Moreover, thanks to the impressive advances undergone in crossed molecular beams (CMBs) and different spectroscopic detection techniques, experimental measurements of the state-to-state differential cross-section (DCS), one of the most sensitive indicators of the underlying reaction dynamics, is now possible for some reactions [5–7]. From a theoretical point of view highly accurate *ab initio* potential energy surfaces (PESs) are currently available for most of the benchmark atom–diatom reactions, thus enabling exact quantum mechanical (EQM) calculations to describe in detail the scattering dynamics of these processes. There also exist precise theoretical methods to identify the different existing reaction mechanisms on a particular reactive collision. As an example, the application of a plane wave packet (WP) approach [8] has made possible the separate calculation of the time evolution of the DCS associated to essentially different processes occurring in the $F + HD$ [9, 10] and $H + D_2$ [11, 12] reactions. In both cases it was possible to study the competition between a direct mechanism and some other reaction pathway which appeared with some delay with respect to the beginning of the reaction. In fact, this delayed mechanism was assigned as responsible of the previously observed quantum dynamical resonance for the $F + HD$ system [13–15]. The origin of an analogous feature in the $H + D_2$ case, initially the subject of an intense discussion [11, 16, 17], seems to lie in the existence of interferences of quantum bottleneck states [18].

Atom–diatom collisions are usually classified into two different types of processes. On one hand, for some collisions, the reaction is the result of a direct mechanism in which the atom attacks the diatom in a very fast way leading to the breakage of the diatomic bond within a very short time interval. These are called *abstraction* reactions. On the other hand, the responsible dynamical mechanism of the *insertion* reactions yields the formation of an intermediate complex between the reactants and products, with the three atoms linked together at very short interparticle distances

for a relatively long period of time. The dynamics associated to each kind of reaction is therefore completely different, and a precise identification of the dominating reaction pathway during the collision thus constitutes a fundamental step in order to understand the overall physics of the process. Insertion reactions are characterized by the existence of deep potential wells which support many bound and quasibound states associated with the previously mentioned intermediate complex. This fact makes EQM calculations in general extremely expensive in terms of computing time. The possibility of applying approximate and computationally less demanding methods becomes of great interest to tackle the investigation of these reactions. In this sense, a statistical treatment of insertion reactions may be justified by both the already mentioned large number of existing bound states and resonances and the long time scale characteristic of these processes, which allows the randomization of the reaction energy among the internal modes of the intermediate complex.

In this paper, recent studies on different types of atom–diatom collisions using a statistical quantum method (SQM) developed some years ago [19, 20] are reviewed. During the past few years, a great number of atom–diatom reactive collisions have been studied by means of this statistical approach. Extensive comparisons with both experimental and EQM results show the feasibility of such an approximate scheme to investigate the dynamics of these insertion reactions. First, results for $X + H_2$ collisions where X is a non-metallic electronically excited atom ($C(^1D)$, $N(^2D)$, $O(^1D)$ and $S(^1D)$) are discussed. In principle, these are processes which are thought to proceed mainly via the formation of an intermediate complex. An example of an ion–diatom reaction, the H_3^+ system, is also considered in this review. Finally, special interest is shown for those collisions for which competition between insertion and abstraction mechanism has been previously reported. An example of this type of process is found for the reaction of O_2 with an H atom. The SQM provides clear insights to distinguish to what extent the insertion mechanisms are present in the overall dynamics of the reaction.

In section 2, an extensive review of the numerous previous statistical treatments employed in the study of atom–diatom reactions is presented. Moreover, the most significant aspects about the theory of the method are also discussed. The study of each reaction included in the present review is preceded by a brief introduction which contains information about previous investigations on the corresponding collision. This survey through the existing literature has been carried out giving special emphasis to two main aspects:

(i) the information regarding the reaction mechanism; and
(ii) the possible existence of previous applications of statistical approaches.

Finally, the results are followed by a summary.

2. Theory

Statistical approaches have been widely applied to the study of reactive atom–diatom collisions. This section is devoted to presenting an overview of some of these statistically

inspired theories which have preceded the present SQM. In addition, the most relevant aspects of the theory of the method are discussed in some detail in section 2.2.

2.1. *Previous statistical treatments*

Statistical techniques to study complex-forming reactions have been widely applied for a long time. The theoretical foundation of most of the earlier work in this subject can be found on previous studies within the nuclear physics field [21, 22]. In some cases, nuclear reactions in which a particle, a neutron for example, collides with a target nucleus may be studied considering the production of a compound nucleus, whose decay products are finally the global reaction products. In those statistical theories the formation of such an intermediate nucleus and its decay were treated as independent events. An interesting consequence of the statistical assumptions considered for these processes is the symmetry of the predicted angular cross-sections with respect to the $\theta = 90^\circ$ centre of mass (CM) scattering angle direction, usually with peaks in the forward and backward directions. This feature was concluded to be directly connected with three assumptions [23]:

(i) the reaction proceeds through the compound nucleus;
(ii) several overlapping levels are excited in that nucleus; and
(iii) random phases of the levels are excited by different partial waves.

Thus, any departure from this forward–backward symmetry was understood to be due to the existence of direct interactions which do not lead to the formation of the compound nucleus. A great deal of effort was made in order to test the statistical theory on different nuclear reactions [24, 25], but although the statistical treatment seemed to be corroborated by the symmetrical experimental angular distributions of protons from (d, p) reactions in Ni nuclei [26], questions about a possible violation of the statistical assumptions to justify the lack of symmetry on the angular distributions were also pointed out [23].

These ideas were directly adapted to the context of reactive molecular collisions [27–29]. Symmetrical features found on CMB angular distributions started to be subsequently attributed to the existence of statistical complexes with its total angular momentum partitioned mainly between the initial and final orbital momenta, l and l', respectively [30–35]. Rotational distributions of OH split from water by electron impact were simulated by means of a statistical model including angular momentum conservation requirements [36]. The main assumption in this treatment is that the excess energy contained in the excited water molecule is randomly distributed among the vibrational and rotational degrees of freedom of the product fragments before they separate from each other beyond a certain distance. Expressions to theoretically simulate experimental product distributions such as velocity, rotational, vibrational and angular distributions, were obtained within the framework of a statistical complex model [31, 35, 37, 38].

Phase-space theory (PST), initially developed in the mid-1960s [39–44], constitutes another example of a statistical treatment of molecular processes mediated by the formation of a collision complex. The main postulate of the theory is that the decomposition of such a complex is governed by the phase space available to

each product under conservation of angular momentum and energy [39]. The total cross-section for the process between a specific initial channel α and a final channel β, statistically divided among the various products of the fragmentation, was written as [44]:

$$\sigma(\{\alpha\} \rightarrow \{\beta\}) = \frac{\pi\hbar^2}{2\mu_\alpha E_\alpha}(2L_\alpha + 1)\sum_J (2J+1)\frac{n[\{\alpha\}, J]\, n[\{\beta\}, J]}{N_{\text{tot}}(J)}, \tag{1}$$

where μ_α, L_α and E_α are the reduced mass, the orbital angular momentum and the relative translational energy, respectively, in the channel α and J is the total angular momentum. Interestingly, the cross-section of equation (1) is expressed in terms of the number of states available in the channels α and β ($n[\{\alpha\}, J]$ and $n[\{\beta\}, J]$, respectively) which can form, or be formed from, a complex of a specified energy and angular momentum, and of the total number of available states at those values of E and J, $N_{\text{tot}}(J)$. With this method, the final product distributions and cross-sections for both ion–molecule reactions $(\text{Rg} + \text{HD})^+$ [41] and neutral processes such as $\text{K} + \text{HBr}$ [42] were tested against experimental results. The statistical method was then extended to obtain angular distributions, and theoretical predictions for DCSs were compared for the $\text{Rb} + \text{CsCl}$ reaction with experiment [45].

In a unifying summary of the previous work, Miller [46] derived some of the key ingredients of modern versions of statistical models. In the calculation of a general expression for the overall transition between an initial, i, and a final, f, state, the contribution from complex-mediated processes was separated of the direct $i \rightarrow f$ transition. The former was expressed, in a similar way to equation (1), as the product between the probability of formation of the collision complex from the channel i and the probability of the complex to fragment through the channel f. The state-to-state probability was obtained after an energy average which precludes the model from providing any information on the possible resonance structure of the reactive process under study.

Transition state (TS) (or activated-complex) theory [47–54] itself has been categorically pointed out not to provide a description of collision-complex processes [51, 55, 56]. In fact, it has been described as a 'direct crossing' barrier theory [55] where the statistical assumption is applied to the equilibrium nature of the reactants located at one side of the barrier but not to the dynamics of the reaction. Within the context of a classical mechanical trajectory calculation, the TS treatment involves the existence of a dividing surface between reactant and product configuration space through which no trajectory passes more than once. The formation of a collision complex corresponds, on the contrary, to a situation in which trajectories undergo back and forth oscillations through the interaction region where the complex is assumed to exist. Thus, this 'trapped' trajectory [56, 57] will eventually cross that dividing surface several times. Statistical theories which describe 'complex' reactions require the existence of two dividing surfaces to separate the complex region from reactants and products, respectively. The probability is then calculated in terms of the microcanonical fluxes through these two surfaces [58, 59]. Remarkable efforts to bring together the TS theory suitable for direct reactions and previous statistical models conceived

for collision processes which proceed via the formation of an intermediate complex are Miller's unified statistical theory [58, 59] and the Pollak–Levine maximum entropy derived statistical theory [60]. Within the unified theoretical framework of the former approach, a third surface in between the two others is defined. The probability that the system crosses this middle surface repeatedly is calculated and used with fluxes through the other outer surfaces to extract the total reaction probability. The theory of Pollak and Levine, on the other hand, is based on the idea of the applicability of statistical theories to any type of dynamics, the only distinction between the different limits (direct versus complex) being the nature and value of the informative constraints to consider [60]. Some other statistical theories based in trajectory approaches have been proposed. In the theory of Wagner and Parks [61], for instance, the issue of a precise implementation of different spatial strong coupling regions was extensively discussed. The 'middle ground' between TS-like theories and the PST approach by Light and collaborators has also been proposed in treatments in which the statistical nature of the process may be parametrically varied [62].

Different TS theory-based approaches for unimolecular [63, 64] and bimolecular processes with formation of transient complexes [38, 51–54] have been developed. The key idea behind these approaches is that the energy is randomly distributed among the different degrees of freedom of the complex in a period of time usually much smaller than its average lifetime. This long-time behaviour can then be described by means of a statistical treatment such as the Rice–Ramsperger–Kassel–Marcus (RRKM) theory [49, 65, 66]. In this sense, characteristic times of the different reaction steps and energy distribution mechanisms are directly linked [67]. It is expected, for instance, that the formation of a long-lived intermediate complex and the equal participation of all modes of that species in product formation may correspond to a statistical partitioning of the energy. On the contrary, this is not the case for a rapid and direct process. A similar non-statistical energy partitioning may be found in reactions for which, despite the possible formation of long-lived complexes, specificity appears due to topological features on the exit channel PES.

Product distributions are, within this statistical formalism, determined primarily by the statistical densities of rotational and vibrational states of the TS. Thus the identification of two limiting forms for the TS, loose and tight, is relevant to understanding the final outcome of the fragmentation process [49, 54]. In fact, loose TS theory with full angular momentum restrictions was found to be equivalent to the PST mentioned above [54]. TS and PST based statistical alternatives have been recently used to study both unimolecular [68–72] and bimolecular processes [73–75].

The reaction rate for a collision which proceeds via the formation of a long-lived complex can be written in terms of the RRKM rates for dissociation of the complex to products and reactants, k_p and k_r, respectively. In particular, the rate of the first barrier crossing from the reactants' valley is calculated by TS theory and the probability of final fragmentation to products is the ratio between k_p and the total rate of dissociation $k_r + k_p$. The rate for the overall process is expressed as [55]:

$$k(E) = \frac{N^{\ddagger}(E - E_{0i})}{h\rho(E)} \cdot \frac{N^{\ddagger}(E - E_{0f})}{N^{\ddagger}(E - E_{0i}) + N^{\ddagger}(E - E_{0f})}, \tag{2}$$

where $\rho(E)$ is the density of states of reactants before the collision, the entrance and exit barrier heights are denoted by i and f, respectively, and $N^{\ddagger}(E-E_0)$ is the number of internal states of the complex at the TS in each case.

In the statistical adiabatic channel model (SACM) of Quack and Troe [76], localized activated complex configurations are replaced by 'open reaction channels' which correlate reactant and product states. A universal function is assumed for interpolating the dependence on the reaction coordinate of the frequency of those vibrational modes correlating with modes of the separated fragments as we move from the molecule to the fragments. The adiabatic character of the theory is related to the 'conservation' of the modes which do not disappear in the crossing of the barrier on the way from reactants to products, while the statistical nature has to do with the energy redistribution in the molecule and in the transitory modes [55]. The final expression for the rate constant of the fragmentation process adopts the following RRKM form:

$$k(E,J) \simeq \frac{W(E,J)}{h\rho(E,J)}, \tag{3}$$

where $W(E,J)$ is the sum of the open adiabatic reaction channels. Examples of early applications to unimolecular processes of the SACM, which was also extended to bimolecular reactions [77], were the calculations of product state distributions for the dissociations of ClNO and NO_2 [78].

A lot has been discussed about the exact correspondence between the statistical behaviour of the collisional process and the actual formation of an intermediate complex [46, 79]. In some cases, as in the PST approaches of Light and collaborators, the statistical limit is considered as a result of the existence of such a collision complex. However, this limit may arise from mechanisms other than complex formation [29, 80, 81]. The apparent success of random phase approximations for elastic atom–atom collisions leads us to conclude that the existence of such a complex is not a necessary prerequisite for the validity of statistical treatments [79]. The study of the statistical features of the S-matrix for molecular collisions by Levine and Johnson concluded that even in the absence of resonances, the statistical approximation for calculating probabilities and cross-sections is justified by the rapid energy variation found for the elastic phases [79].

A similar controversy was originated by the reproduction by means of a RRKM simulation method [82–85] of experimental (both LAB and CM) angular and energy distributions for $O+I_2$ and $O+Br_2$ [86], and the rotational distributions for the $O(^3P)+HBr$ [87] and $O(^3P)+HCl$ [88] collisions. In particular, the good agreement found with experimental results for the reactions between the ground electronic state of atomic oxygen, $O(^3P)$, with the HX diatoms seems to contradict the abstraction mechanism expected for these processes, characterized by repulsive PESs. The overall description provided by the statistical method which assumes the formation of an intermediate complex during the reaction opens questions about the actual mechanism of these sorts of collisions, and definitive conclusions have not yet been established [89]. On the other hand, to complicate things even more, theoretical treatments initially

designed for collision-complex-forming processes [38] turned out to be of some help for reactions mediated by short-lived complexes [90], in apparent disagreement with previous conclusions on the validity of such methods [58, 91].

It may be concluded that the main basic aspects of any statistical theory for reactive scattering collisions could be summarized in the following points:

(i) Lack of correlation between the formation process of the 'compound complex' and the mode of its decomposition apart from the conservation laws for energy, total angular momentum and linear momentum [44]. In particular, this enables the construction of the state-to-state reaction probability for the process between the initial state of the reactant channel and the final state of the product channel as the product of separate probabilities accounting for the formation of the intermediate complex and its fragmentation.

(ii) The definition of the region where the complex is supposed to exist. This may involve the selection of the proper range of angular momenta or impact parameter contributing to a particular channel [38, 40, 92], or the precise location where the complex is assumed to exist. This complex region, which may or not be understood as the strong coupling region [60], can also be isolated by the definition of dividing surfaces [58, 59]. Minimum interparticle distance [93] or energy [94] criteria have also been used in trajectory calculations to describe the region where the complex is assumed to be formed.

(iii) The calculation of the individual probabilities for the complex to be formed or to fragmentate. Different possible values may be assumed for those probabilities: zero or unity depending on whether or not the value of the orbital angular momentum L corresponding to the state of the complex is allowed [44] or whether or not the parameter impact exceeds a certain value [46], the proportionality factor to the impact parameter [31, 38, 43], the number of energetically open states, etc. These probabilities, as mentioned above, may also be extracted from the microcanonical flux through the surfaces which divide the configuration space between reactants, collision complex and product regions [58, 59].

(iv) The satisfaction of detailed balancing, ensured by the symmetry of the probabilities of the $i \rightarrow f$ and $f \rightarrow i$ processes [19, 40].

2.2. *The statistical quantum method*

The goal of this section is simply to supply the most relevant theoretical features of the method. A more detailed discussion on the foundations of the SQM can be found in the original papers where the model was introduced [19, 20] and its applications to insertion processes [95–98]. The main assumption required for the model to be valid is the need of the formation of an intermediate complex during the process of the atom–diatom reaction. The lifetime of such a collision complex is moreover considered to be long enough to justify the study of the whole process by treating its formation and subsequent fragmentation as independent events. Having fulfilled these requirements it is then possible to approximate the state-to-state reaction probability between an initial $vj\Omega$ state in the arrangement α and a final $v'j'\Omega'$ state in

the arrangement α', for a total angular momentum J and a parity eigenvalue I, in the helicity representation as

$$|S^{IJ}_{\alpha' v' j' \Omega', \alpha v j \Omega}(E)|^2 \simeq \frac{p^{IJ\alpha'}_{v' j' \Omega'}(E) p^{IJ\alpha}_{v j \Omega}(E)}{\sum_{\alpha'' v'' j'' \Omega''} p^{IJ\alpha''}_{v'' j'' \Omega''}(E)}, \tag{4}$$

where v and j are the diatomic vibrational and rotational quantum numbers, respectively, and Ω is the modulus of the projection of the diatomic rotational angular momentum on the atom–diatom axis. In equation (4), $p^{IJ\alpha}_{vj\Omega}$ and $p^{IJ\alpha'}_{v'j'\Omega'}$ can be understood, respectively, as the capture probability or probability of forming the collision complex from the reactant channel $vj\Omega$ and as the capture probability from the product channel $v'j'\Omega'$, i.e. the probability for the collision complex to decay to that product channel, respectively. The capture probabilities can be written as

$$p^{IJ\alpha}_{vj\Omega}(E) = 1 - \sum_{v'j'\Omega'} |S^{IJ\alpha}_{v'j'\Omega', vj\Omega}(E)|^2 , \tag{5}$$

where the sum runs over all the energetically open channels. Equation (5) expresses the fact that the lack of unitarity of the scattering matrix $S^J(E)$ with respect to the usual inelastic scattering calculation is attributed to capture by the collision complex [19]. The scattering matrix in the above expression is thus obtained by solving for each chemical arrangement the corresponding close-coupled equations [19]. The solution of those equations is performed by means of a time independent (TI) log derivative propagation [102] between the corresponding asymptotic region and a specific capture radius which defines the region where the complex is assumed to exist. This is undoubtedly one of the aspects which makes the SQM economize on the computational requirements, since the definition of such a capture radius implies the neglect of the region of the potential well. Thus, the precise description of the large number of bound and resonant states supported by the PES is no longer required within the SQM framework. In EQM calculations, on the contrary, the use of extremely large radial grids or too long propagation times is needed. In the present review, results have been obtained within the centrifugal-sudden (CS) approximation [99–101]. Deviations from calculations carried out within the more rigorous coupled-channel scheme were found not to be significantly large [97].

Another key feature which distinguishes the SQM from previous statistical approaches is that the evaluation of the capture probabilities $p^{IJ\alpha}_{vj\Omega}$ is carried out in the most rigorous possible way. No simplification on the long-range forces is introduced and standard chemically accurate *ab initio* PESs are used. In addition, the capture theory of Clary and Henshaw [103] is employed in the calculation of these capture probabilities. Although the SQM used in the studies reviewed in this work is based on a TI scheme, recent examples of a WP version of the model have been reported [104–107].

It is worth mentioning here that the simulated reaction probability obtained with the SQM approach involves an energy average [46] which precludes the model from providing any information about the possible existing resonant structure of the

EQM result. The best the method can do is to produce an average description of the exact reaction probability.

An illustrative picture of the theoretical basis of the SQM is shown in figure 1. The capture radii for the reactant and product valleys (r_c and r'_c, respectively) define the intermediate complex or strong coupling region. The calculation is carried out independently in both arrangements from the corresponding capture radius up to the asymptotic regions. Thus, the region which contains the potential well is excluded. As a result of such a calculation, the capture probabilities $p^J_{vj\Omega}$ and $p^J_{v'j'\Omega'}$ from the initial and final states $vj\Omega$ and $v'j'\Omega'$, respectively (schematically shown in figure 1) are obtained.

The statistical state-to-state integral cross-section (ICS) can then be evaluated from the EQM expression

$$\sigma_{\alpha' v' j', \alpha v j}(E) = \frac{\pi}{g k^2_{\alpha v j}(2j+1)} \sum_{IJ\Omega\Omega'} (2J+1) \mid S^{IJ}_{\alpha' v' j' \Omega', \alpha v j \Omega}(E) \mid^2, \tag{6}$$

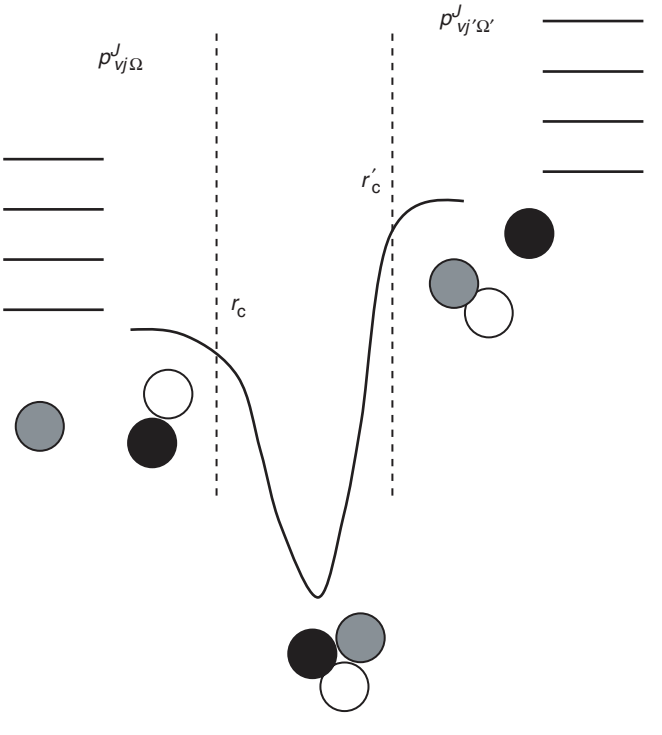

Figure 1. Schematic picture of the basic aspects of the theory of the SQM. The initial $vj\Omega$ and final $v'j'\Omega'$ states from the reactant and product arrangements, respectively, are indicated with horizontal lines. Dashed lines denote the location of the capture radii r_c and r'_c, which define the intermediate complex (or strong coupling) region. The log-derivative propagation to calculate the corresponding capture probabilities $p^J_{vj\Omega}$ and $p^J_{v'j'\Omega'}$ is carried out, independently in the reactant and product valley, from the capture radius to the asymptotic region. This excludes the deep potential well region of this calculation.

with $k^2_{\alpha vj} = 2\mu(E - E_{vj})/\hbar^2$, E_{vj} being the energy of the initial rovibrational state vj of the reactant diatom and g the electronic degeneracy. The reactive probability $|S^{IJ}_{\alpha' v' j' \Omega', \alpha vj\Omega}(E)|^2$ is approximated as equation (4).

The expression for the statistical DCS, once a random phase approximation is invoked, is the following [20]:

$$\sigma_{\alpha' v' j', \alpha vj}(\theta, E) \simeq \frac{1}{8k^2_{\alpha vj}} \frac{1}{2j+1} \sum_{IJ\Omega'\Omega} (2J+1)^2 \left[d^J_{\Omega'\Omega}(\pi - \theta)^2 + d^J_{\Omega'\Omega}(\theta)^2 \right] \times |S^{IJ}_{\alpha' v' j' \Omega', \alpha vj\Omega}(E)|^2 . \tag{7}$$

The presence of the ${d^J_{\Omega'\Omega}}^2$ reduced rotation matrix terms in equation (7) means that statistical DCSs are forced to exhibit symmetrical maximum peaks in the forward and backward scattering directions. Although different reasons as to the origin of this symmetry around 90° have been invoked, in the context of the present statistical method, this feature has to be understood as a clear indication of insertion dynamics.

Statistical predictions for the initially state-selected thermal rate constants can also be obtained by means of the standard expression:

$$k_{vj} = Q^{-1}_{el} \sqrt{\frac{8}{\pi\mu(k_B T)^3}} \int_0^\infty \sigma_{vj}(E) \exp(-E/k_B T) E dE \tag{8}$$

where Q_{el} is the electronic partition function, k_B is the Boltzmann constant and the ICS, $\sigma_{vj}(E)$, is calculated by using equation (6) and summing over all final states v', j'.

In this review examples of some other quantities, such as product laboratory angular distributions (PLADs) and time-of-flight (TOF) distributions, also reproduced by means of the SQM approach, will be shown. The usual procedure to compare with experiment is to obtain theoretical expressions of such magnitudes, originally measured in the laboratory (LAB) angle. Thus, theoretical DCSs derived in the CM frame are transformed into the LAB frame, taking into account the averaging over different experimental conditions and the distribution of initial rotational j states in experiment with their relative reactivity. Theoretical angle-dependent product translational energy (PTE) distributions for each initial j are also used in the simulation.

The present SQM has been recently extended to include the electronic degrees of freedom (orbital and spin angular momenta) of the product fragments to obtain product multiplet-resolved ICSs [108] and rate constants [109].

3. Study of insertion reactions: X + H_2 collisions

The reactions of H_2 with non-metallic electronically excited atoms such as C(^1D), N(^2D), O(^1D) and S(^1D) have been intensively studied. As will be discussed below, great effort has been made in order to characterize precisely the dynamics of these reactions. The interested reader is referred to some of the numerous existing reviews on this subject [5, 6, 110, 111]. As mentioned in the introduction, the present work is

mainly focussed on the knowledge we have on the reaction mechanism and the previous applications of statistical approaches to investigate these collisions.

All the four processes treated in this section are distinguished by the existence of deep potential wells between reactants and products. The values of the depths associated with the corresponding intermediate species XH_2 are, from the lowest to the highest, 4.23 eV for the collision with $S(^1D)$, 4.29 eV for $C(^1D)$, 5.48 eV for $N(^2D)$, and 7.29 eV for $O(^1D)$. Another feature in common is that they are all exoergic processes in which the product asymptotic region lies below that corresponding to the reactants. The degree of exoergicity, however, ranges from 1.33 eV and 1.92 eV for the $N(^2D)$ and $O(^1D)$ reactions, respectively, to 0.26 eV and 0.29 eV for the $C(^1D)$ and $S(^1D)$ collisions. Finally, the $N(^2D) + H_2$ reaction is the only one presenting a small barrier in the entrance channel.

3.1. $C(^1D) + H_2$

Since the earliest *ab initio* calculations, it was clearly manifested that, whereas there exists no barrier for $C(^1D)$ insertion into the H–H bond, linear abstraction does present a barrier [112]. Thus an insertion mechanism is anticipated for the reaction between $C(^1D)$ and H_2 to finally produce $CH(^2\Pi)$. However, the participation of direct abstraction was predicted to augment when the kinetic energy is increased. Subsequent experimental studies on the reaction seemed to confirm these conclusions [113–116]. Rotational population distributions in $CH(v' = 0)$ obtained by means of a laser-induced fluorescence (LIF) experiment were found to be adequately described by thermally averaged statistical predictions [113]. These findings were rationalized in terms of the formation of an intermediate complex CH_2 with a sufficiently long lifetime (of the order of picoseconds [113, 117]) to ensure complete randomization of the reaction energy before the fragmentation to products. No evidence of rotationally cold CH fragments confirmed the absence of an abstraction mechanism.

The preference for CD formation in the reaction of $C(^1D)$ and HD, with values for the branching ratios CD/CH between 1.6 and 1.7 [114, 116], has also been interpreted as a sign of an insertion reaction mechanism. Further support for such a conclusion was the reproduction of the above mentioned values for the CD/CH ratio by means of a RRK calculation based on a collision complex formed following the insertion of the C atom into the H–D bond [114].

These conclusions in favour of an insertion reaction pathway were nevertheless accompanied by the finding of an increase of the abstraction process when the reactant H_2 is vibrationally excited [118]. Moreover, in comparison with the $O(^1D) + H_2$ collision, abstraction was suggested to play a more important role in the $C(^1D) + H_2$ reaction due to the production of a lower rotational energy fraction [114]. Finally the (only qualitative) agreement found between CMB results and PST predictions for the product angular and TOF distributions led authors of [119] to conclude the nearly statistical behaviour for the $C(^1D) + H_2$ reaction.

More recently a large amount of theoretical and experimental work on this reaction has been carried out. The application of quantum approaches has revealed that the dynamics of the process is clearly dominated by the existence of long-lived

resonances [120–122]. Angular DCSs were found to exhibit a symmetrical shape with peaks in the forward and backward directions [123, 124], thus suggesting insertion dynamics. In addition, a quasiclassical trajectory (QCT) calculation, despite not reproducing the polarized DCSs, yielded collision time distributions consistent with long-lived intermediate complexes [124]. Comparison of results obtained by a WP version of the SQM reviewed here with previous experimental distributions and EQM results showed good enough agreement to also sustain the idea of such a reaction mechanism [104, 105].

The SQM calculations, shown in this section for the $C(^1D) + H_2$ collision, have been carried out on the PESs of Bussery-Honvault *et al*. [120].

The initially state-selected reaction probability for the $C(^1D) + H_2(v = 0, j = 0)$ reaction for a zero total angular momentum, $J = 0$, is shown in terms of the collision energy up to $E_c = 0.5$ eV in figure 2. Results from the SQM approach are compared

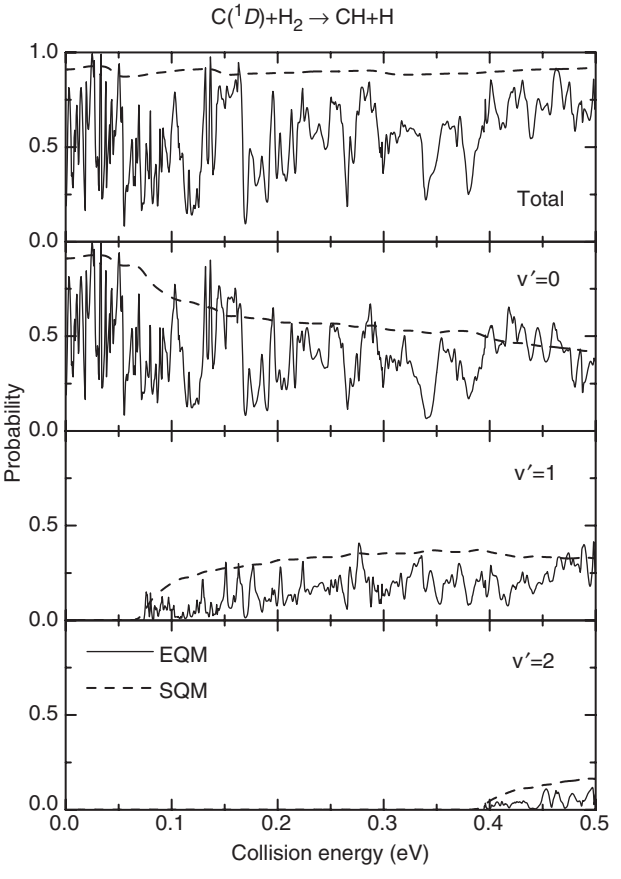

Figure 2. State-to-state selected reaction probabilities for the $C(^1D) + H_2(v = 0, j = 0) \rightarrow CH(v') + H$ for a zero value of the total angular momentum, $J = 0$, in terms of the collision energy E_c. EQM (solid lines) from [120] and SQM (dashed lines) probabilities are compared for $v' = 0$–2. Probabilities for all final vibrational states are shown in the top panel.

with previous EQM results [120] when either the final vibrational state CH(v') is specified or the sum over all the final vibrational manifold is considered. As mentioned in section 2.2, the statistical method cannot reproduce the resonant structure of the EQM result. Thus, no information about the numerous narrow peaks exhibited in the EQM reaction probability are described by the SQM. The average description provided by the statistical prediction seems to overestimate both total (on the top panel) and final vibrational-state selected EQM reaction probabilities. The reactivity of the collision of $C(^1D)$ with H_2 is apparently not as large as expected with a capture theory approach. The reaction thresholds for the reaction to produce vibrationally excited CH fragments ($v' = 1$ and 2) are nevertheless well described in the statistical result.

Fortunately, the situation improves a lot when the comparison with the EQM results is made for larger values of the total angular momentum, $J > 0$. As shown in the top panel of figure 3, where the opacity function for the $C(^1D) + H_2$ reaction at $E_c = 80$ meV is shown, the statistical total reaction probabilities get closer to the exact result as J increases. This could be rationalized by the larger number of both initial and final states accessible (assuming that the total energy is enough to overcome the corresponding centrifugal barriers) from the intermediate complex in comparison with the $J = 0$ case. In order to obtain accurate predictions for quantities such as

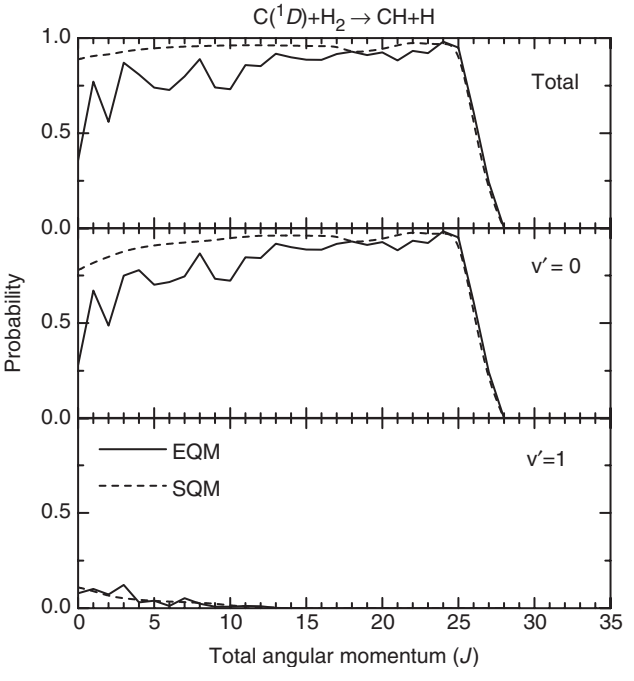

Figure 3. Opacity functions or reaction probabilities in terms of the total angular momentum J for the $C(^1D) + H_2(v = 0, j = 0)$ collision at 56 meV collision energy. EQM results (solid line) from Honvault and Launay are compared with the statistical probabilities (dashed line) for the total reaction (in the top panel) and the $v' = 0$ and 1 final state resolved process in the middle and bottom panels, respectively.

cross-sections, a good description of probabilities for high values of J is crucial. Moreover, the correct reproduction of the high J tail of the opacity functions is probably much better than what one may expect from classical capture theories.

An example of this predicted good performance of the SQM to produce accurate cross-sections is given in figure 4. In this figure, vibrationally resolved rotational ICSs obtained at the same collision energy of 80 meV with the SQM approach and a previous EQM calculation [123] are compared. The good accord between both theoretical methods to predict hot rotational distributions is an indication of the insertion-like nature of the reaction. The production of CH in the excited vibrational state $v' = 1$ is almost negligible and does not involve too many final rotational states j'. Vibrationally resolved ICSs are obtained by summing on all final rotational states for each v' level. Comparison of EQM and SQM values for these cross-sections with an initial rotation on the H_2 diatom of $j = 0$ and 1 is shown in table 1. The agreement between the exact and statistical calculation is quite good for both initial rotational states. In particular, as expected from the comparison in figure 4 of the state-to-state ICSs for the $C(^1D) + H_2(v = 0, j = 0) \rightarrow CH(v' = 1, j') + H$ reaction, identical results are predicted by both theoretical approaches.

Given this result, it is not then surprising to find statistical DCSs in a good agreement with EQM results. Figure 5 shows DCSs at the same collision energy for the $C(^1D) + H_2(v = 0, j = 0, 1)$ processes. The statistical angular cross-section gives an excellent average description of the forward–backward symmetry exhibited by the EQM result. At the same time, sideways scattering is correctly well described by the SQM approach. The accord seems to be not as good for the $j = 1$ DCS also included in figure 5. The EQM cross-section displays some deviation from complete

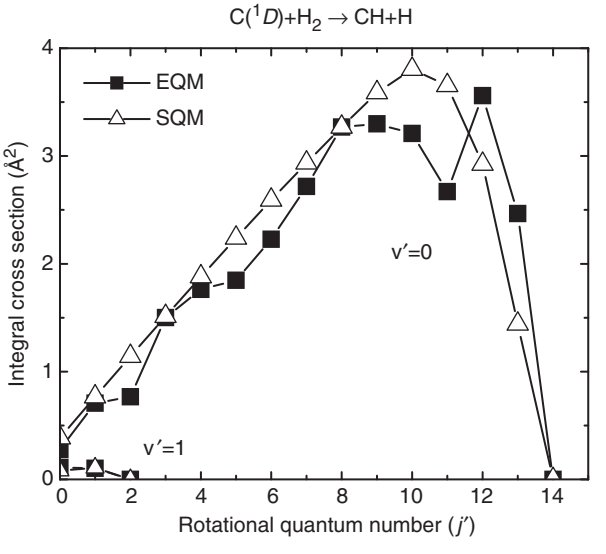

Figure 4. Vibrationally state-resolved rotational ICSs for the $C(^1D) + H_2(v = 0, j = 0) \rightarrow CH(v', j') + H$ reaction at $E_c = 80$ meV collision energy. Results for $v' = 0$ and 1 obtained by means of an EQM calculation [123] (solid squares with lines) are compared with the SQM predictions (empty triangles with lines).

symmetry around the 90° direction, showing some preference for the backward scattering ($\theta = 180°$). Thus, whereas the accord with the maximum peak at the forward direction ($\theta = 0°$) of the EQM DCS is relatively good, the SQM prediction of the cross-section at the backward direction remains too low compared to the exact result.

Table 1. Total σ and vibrationally resolved $\sigma_{v'}$ ICSs for the $C(^1D) + H_2(v = 0, j = 0, 1)$ reaction at a collision energy of $E_c = 80$ meV. EQM results have been taken from [123]. Cross-sections are given in Å^2.

Method	Total	$v' = 0$	v′=1
EQM $j = 0$	30.49	30.28	0.21
SQM $j = 0$	32.29	32.08	0.21
EQM $j = 1$	30.19	29.44	0.75
SQM $j = 1$	31.81	31.14	0.67

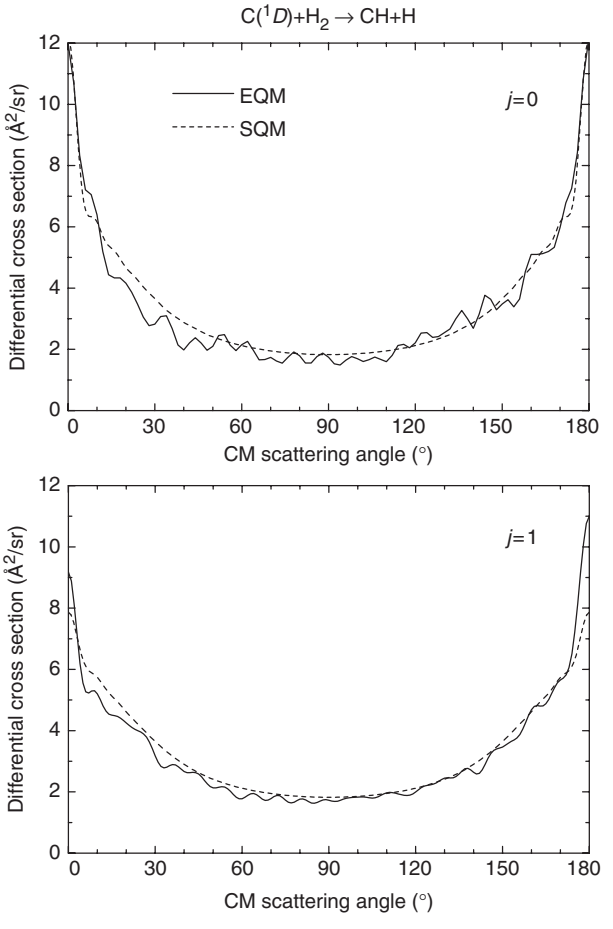

Figure 5. DCSs for the $C(^1D) + H_2(v = 0, j)$ reactions at $E_c = 80$ meV. EQM results from [123] (solid line) are compared with SQM results (dashed line) for $j = 0$ (top panel) and $j = 1$ (bottom panel).

Considering the failure of the QCT approach to describe the dynamical features of the DCS [123], the $C(^1D) + H_2$ reaction illustrates the need for QM methods, such as the SQM, as an alternative to an exact calculation. In general isotope substitutions of H by a heavier atom such as D, makes the corresponding EQM calculation significantly more complicated in computational terms. Therefore, the possibility of performing accurate QM statistical calculations turns out to be of crucial importance. In this sense, the SQM has been applied as the QM approach in a theory versus experiment comparison on the $C(^1D) + D_2$ reactive collision [96].

Figure 6 shows the comparison between CMB experimental and statistical LAB distributions for the $C(^1D) + D_2$ reaction at $E_c = 160\,\text{meV}$ ($15.5\,\text{kJ mol}^{-1}$). The agreement between experiment and theory is quite good, and the only discrepancies seem to have their origin in a larger contribution from the $v' = 1$ vibrational product state (dotted line in figure 6) predicted by the calculation in comparison with the CMB measurement. The accord with experiment extends to the TOF distributions, as shown in figure 7. It is only for the two LAB angle values $\Theta = 22^\circ$ and 26° that some slight discrepancies could be pointed out. In fact, the only serious disagreement found in [96] is between the best-fit CM angular distributions and the SQM DCSs. The statistical angular distribution displays peaked forward–backward symmetry similar to that obtained for the $C(^1D) + H_2$ reaction (see figure 5) whereas a less pronounced ratio between the sideways scattering direction and the peaks at the extreme cases of $\theta = 0^\circ$ and $\theta = 180^\circ$ is shown in the experimental distribution. In this sense it is interesting to remark that a similar lack of accord was reported between the EQM DCSs and the experimental angular distribution in a previous study on the $C(^1D) + H_2$ reaction [124]. Given the good description provided by

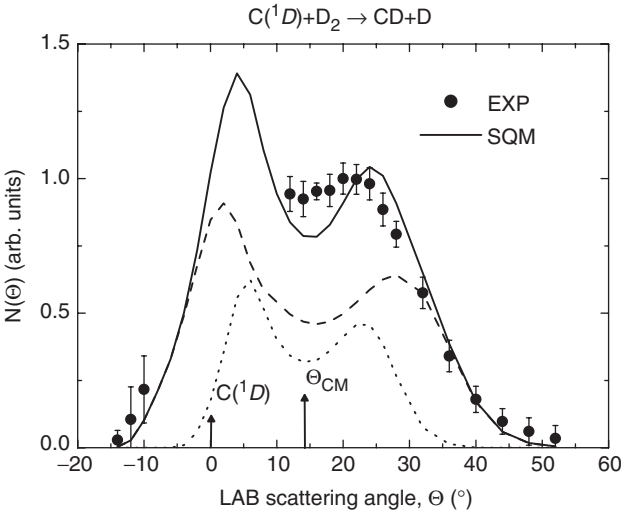

Figure 6. PLADs from the reaction $C(^1D) + D_2$ at $E_c = 160$ meV. SQM results (solid line) are compared with experiment from [96] (black circles and error bars). Contributions from the $v' = 0$ and 1 in the SQM calculation are shown separately with dashed and dotted lines, respectively.

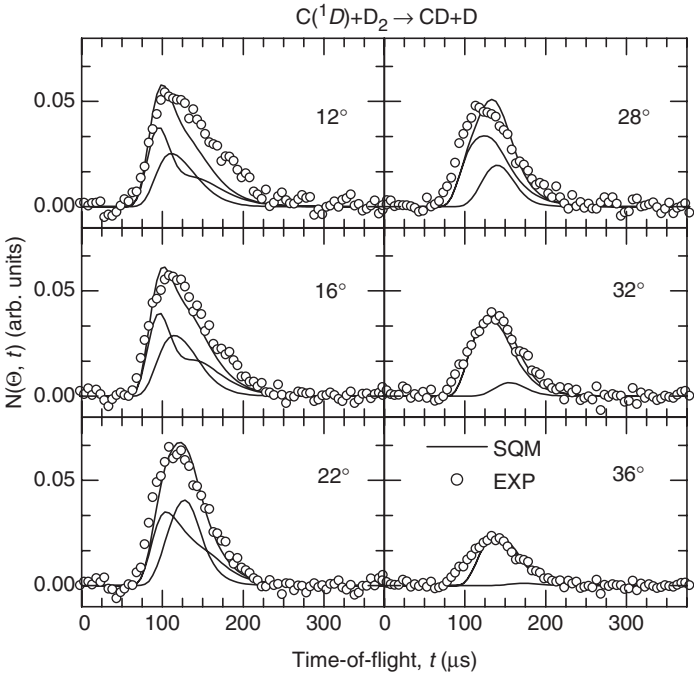

Figure 7. TOF distributions for the reaction $C(^1D) + D_2$ at $E_c = 160$ meV. SQM results (dashed lines) are compared with experimental CMB measurements (points) for the LAB angle values $\Theta = 12^\circ$, 16° and 22° (in the left panels), and 28°, 32° and 36° (in the right panels). Contributions from the $v' = 0$ and 1 for the statistical calculation are also included.

the SQM approach to reproduce the EQM DCS, it is tempting to imagine that a possible EQM calculation on the collision between a C atom and D_2 might be at the same level of disagreement with the CMB result.

Interestingly, the predicted participation of excited PESs in the $C(^1D) + H_2$ reaction [115] has been recently found to yield dynamical features which may not correspond to an insertion reaction pathway [125]. On one hand, a strongly marked preference for a forward scattering direction on the second excited $1\,^1A''$ PES precludes the DCSs from exhibiting the forward–backward symmetry characteristic of insertion processes. On the other hand, the QCT calculation shows that the distribution of classical collision times is much narrower on the excited PES than on the ground PES, extending to significantly lower values, thus indicating that formation of a long-lived intermediate complex is much more unlikely in the excited PES dynamics. It is therefore expected that statistical treatments do not provide a valid description of the dynamics in this case. A nice confirmation of the non-insertion-like nature of the $C(^1D) + H_2$ collision on the $1\,^1A''$ PES is the comparison shown in figure 8 of the QCT and EQM DCSs from [125] with the SQM prediction at $E_c = 80$ meV for the case of no initial rotation, $j = 0$, on the H_2 diatom. The statistical distribution, which seems to underestimate the forward peak of both the QCT and EQM results, gives the wrong prediction for the backward intensity. The QCT approach, on the contrary, accounts for the correct

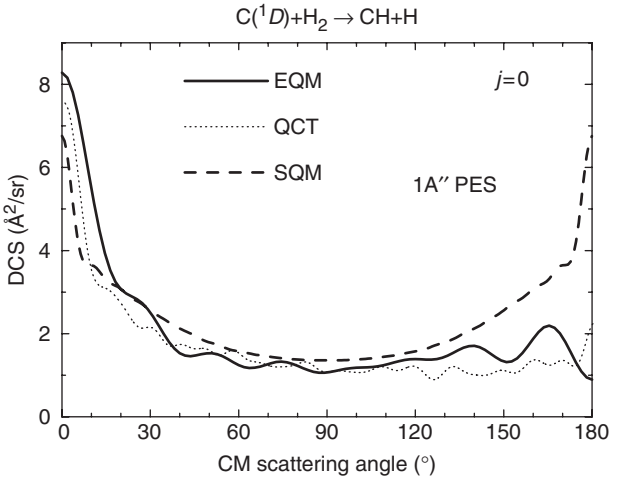

Figure 8. Theoretical DCSs for the reaction $C(^1D) + H_2(v = 0, j = 0)$ at $E_c = 80$ meV on the second excited $^1A''$ PES. EQM (solid lines) and QCT (dotted lines) results are taken from [125]. The SQM prediction is given as the dashed line.

deviation from the insertion mechanism found on the excited PES. In addition, values predicted by the SQM for the total ICS ($\sigma = 26.54\,\text{Å}^2$), the vibrationally resolved ICSs ($\sigma_{v'=0} = 23.34\,\text{Å}^2$ and $\sigma_{v'=1} = 3.20\,\text{Å}^2$) and the $(v' = 1)/(v' = 0)$ ratio (0.137) at that collision energy are in clear disagreement with both the EQM ($17.04\,\text{Å}^2, 16.66\,\text{Å}^2$, $0.38\,\text{Å}^2$ and 0.023, respectively) and QCT ($19.78\,\text{Å}^2, 19.14\,\text{Å}^2, 0.64\,\text{Å}^2$ and 0.033, respectively) results [125]. The origin of such a discrepancy may be the extra intensity found in the backward direction of the statistical DCS shown in figure 8.

3.2. $N(^2D) + H_2$

The reaction of $N(^2D)$ with H_2 has, besides $O(^1D) + H_2$, been one of the $X + H_2$ processes reviewed in this section for which more attention has been attracted in order to elucidate the precise dynamics of the collision. In a early experimental study inverted product vibrational distributions with peaks toward high v' levels were reported [126]. This product distribution, in which $NH(v' > 0)$ vibrational states were populated more quickly than the ground vibrational state, is indicative of a direct abstraction mechanism. In fact a statistical analysis yielded hotter and more excited distributions than the experimental result [126]. The only theoretical calculations capable of reproducing the inversion in the experimental distributions employed adjusted London–Eyring–Polanyi–Sato type [127] or *ab initio* PESs which, despite having a deep well for the perpendicular C_{2v} HNH configuration, also exhibits the lowest barrier for a collinear geometry $C_{\infty v}$ [128, 129]. The situation got a bit more complicated with the rotational and vibrational distributions reported by Umemoto and collaborators [130–132]. The vibrational product ratio $NH(v' = 1)/NH(v' = 0)$, smaller than the extrapolated value obtained in the previous experimental work of Dodd *et al.* [126] and earlier theoretical work [128], and the broad rotational

distributions, led the authors to suggest that both insertion and abstraction processes play an important role on the process.

It was then clear that product distributions were dramatically affected by the description of the C_{2v} and $C_{\infty v}$ barriers. The empirical adjustment performed by Kobayashi *et al*. [133] was followed by the *ab initio* construction of a new PES which exhibits a much lower insertion perpendicular barrier in comparison with the abstraction linear one [134]. QCT [134] and EQM [135] calculations on this PES gave further conclusive evidence on the insertion nature of the $N(^2D) + H_2$ reaction. In addition, new experimental investigations on both the $N + H_2$ [136] and $N + D_2$ [137, 138] processes confirmed this conclusion. It is therefore well accepted that the dynamics for this process are mainly typical of an insertion reaction and deviations to an abstraction mechanism are only expected at a really high energy regime [139].

The statistical calculations collected here for this work were carried out on the PES by Pederson *et al*. [134].

The reaction probabilities for the initial state-selected $N(^2D) + H_2(v = 0, j = 0) \rightarrow NH + H$ process at $J = 0$ up to a collision energy of about $E_c = 0.225$ eV are shown in the left top panel of figure 9. The presence of a barrier in the entrance channel of the PES of [134] affects the shape of both the EQM and SQM probabilities which exhibit a characteristic threshold. The corresponding thresholds for the reactions to specific final vibrational states NH(v'), also shown in figure 9, are also well described by the SQM. The profile of the EQM probabilities does not exhibit narrow resonance peaks as in the case of the $C(^1D) + H_2$ (see figure 2). The structure in this case is constituted by broader resonances which seem to strongly overlap, precluding the identification of any individual resonance peak. In this case, the statistical predictions do not overestimate the reactivity found in the exact calculation and the only significant discrepancies could be identified for the probabilities of the formation of $NH(v' = 4)$ (in the bottom right panel of figure 8), for which the SQM yields a significantly larger probability.

The good agreement with the $J = 0$ EQM reaction probability (probably better than in the same comparison for the $C(^1D) + H_2$ reaction) is accompanied by a similar nice description of the result of Honvault and Launay for the $J > 0$ probabilities. As shown in figure 10, which displays the opacity function or reaction probability in terms of J at a collision energy of $E_c = 165$ meV, the SQM result only differs slightly from the EQM probabilities for the lower values of the total angular momentum ($J < 10$) but it does provide an almost quantitatively identical result for the higher values of J. At this collision energy, the opacity function is completely determined by the production of the $NH(v' = 0)$ fragment.

Comparison with the EQM opacity functions allows us to advance the likely reproduction of averaged quantities such as cross-sections obtained by means of the SQM. An illustration of these expectations is shown in figure 11, where theoretical rotational ICSs obtained with the EQM calculation of [135] and the present SQM approach at the same collision energy of $E_c = 165$ meV for the production of $NH(v' = 0)$ (in the bottom panel) and $NH(v' = 1)$ (in the top panel) are compared with experimental results by Umemoto *et al*. [131]. Theoretical distributions were rotationally averaged on the $j = 0$ and $j = 1$ states for the H_2 diatom and experimental measurements were scaled to compare with theory. The tendency of the hot EQM

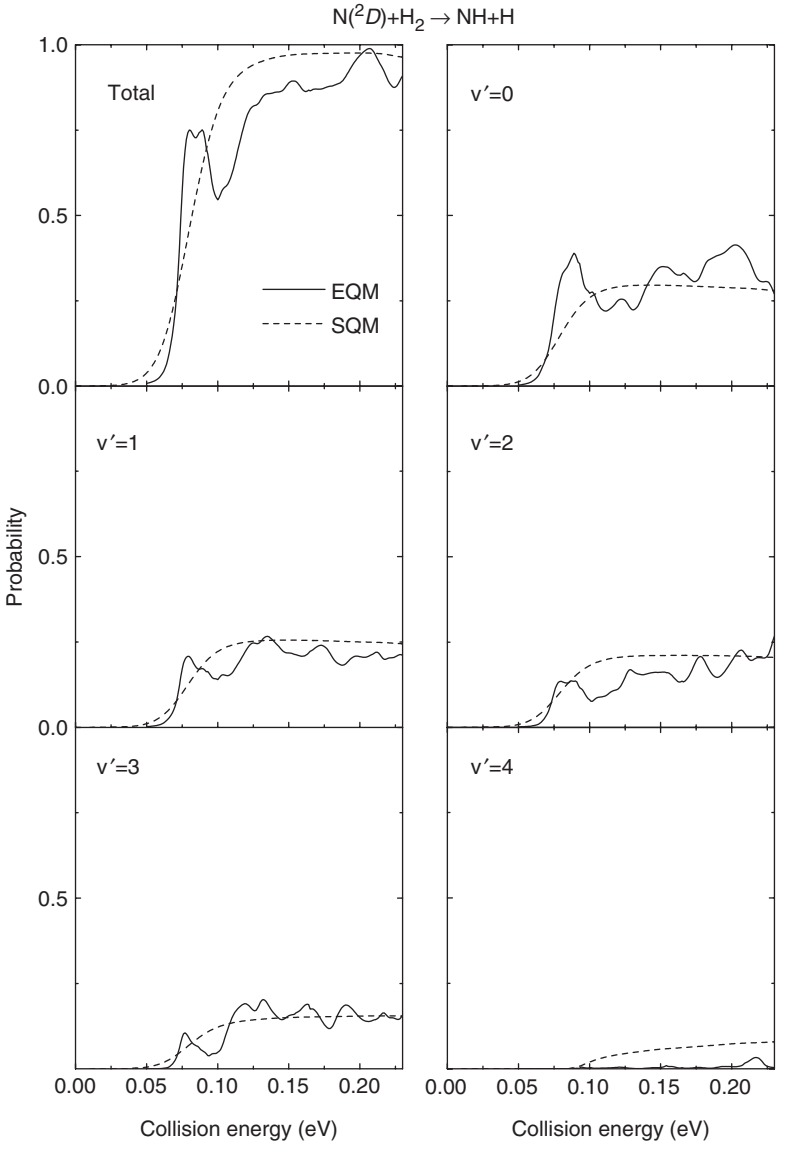

Figure 9. Initial state selected reaction probability for the $N(^2D) + H_2(v = 0, j = 0)$ collision at $J = 0$. EQM results (solid line) by Honvault and Launay for all product vibrational states $NH(v')$ summed are compared in the left top panel with SQM probability (dashed line). Final vibrational state-selected probabilities for the $v' = 0$–4 states are shown in the rest of the panels.

rotational distributions to produce rotationally excited NH fragments partially follows the statistical behaviour. EQM distributions, however, seem to extend slightly more, making the SQM result give an incomplete description of the exact results. The larger deviations are found for the $v' = 0$ final vibrational state, where the maximum

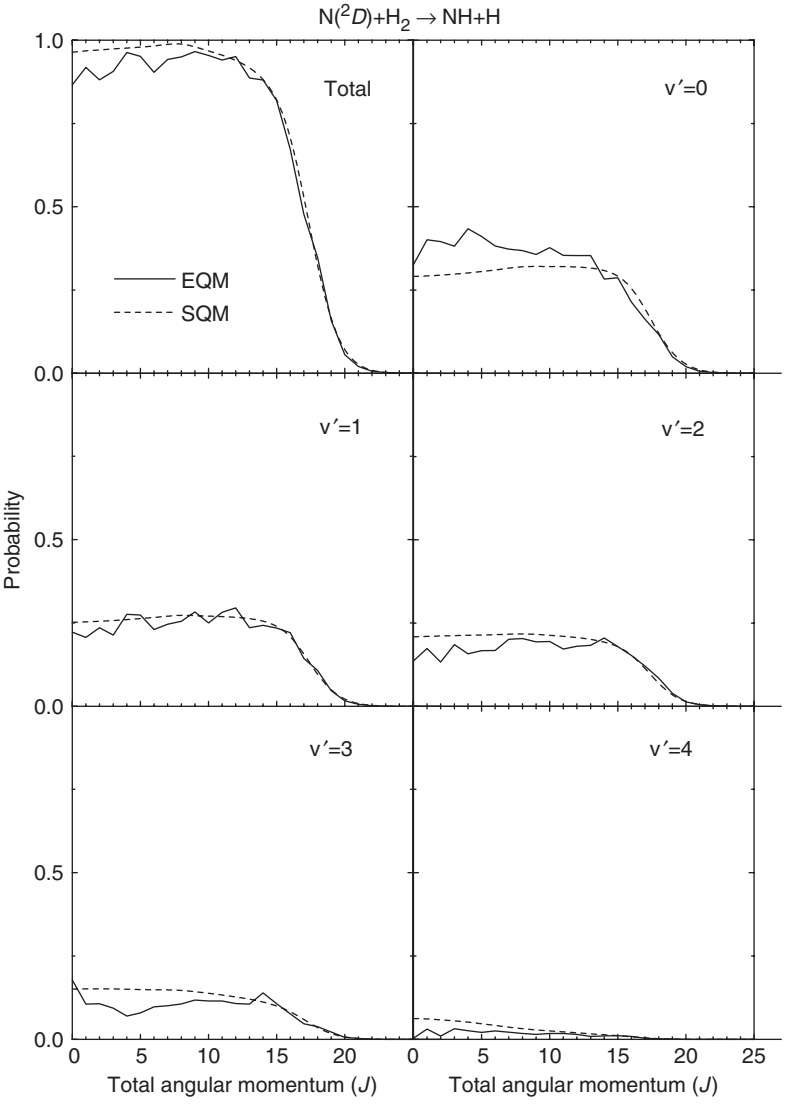

Figure 10. Total (top panel) and final vibrational state selected opacity function for the $N(^2D)+H_2(v=0,j=0) \rightarrow NH(v'=1,2)+H$ reaction at 165 meV collision energy. EQM results by Honvault and Launay are shown as the solid line and SQM predictions as the dashed line.

along the interval $j' = 20$–26 in the exact rotational ICS is not exactly reproduced statistically. The overall comparison is anyway not bad, especially for the case of forming vibrationally excited $NH(v' = 1)$ fragments.

The experimental measurements clearly suggest the formation of rotationally excited product fragments as theory predicts. The increase of the results of Umemoto *et al.* with increasing final rotational state j' found up to $j' = 15$ is in general well described by both theoretical methods in the two cases, $v' = 0$ and 1. For $v' = 0$ the above mentioned

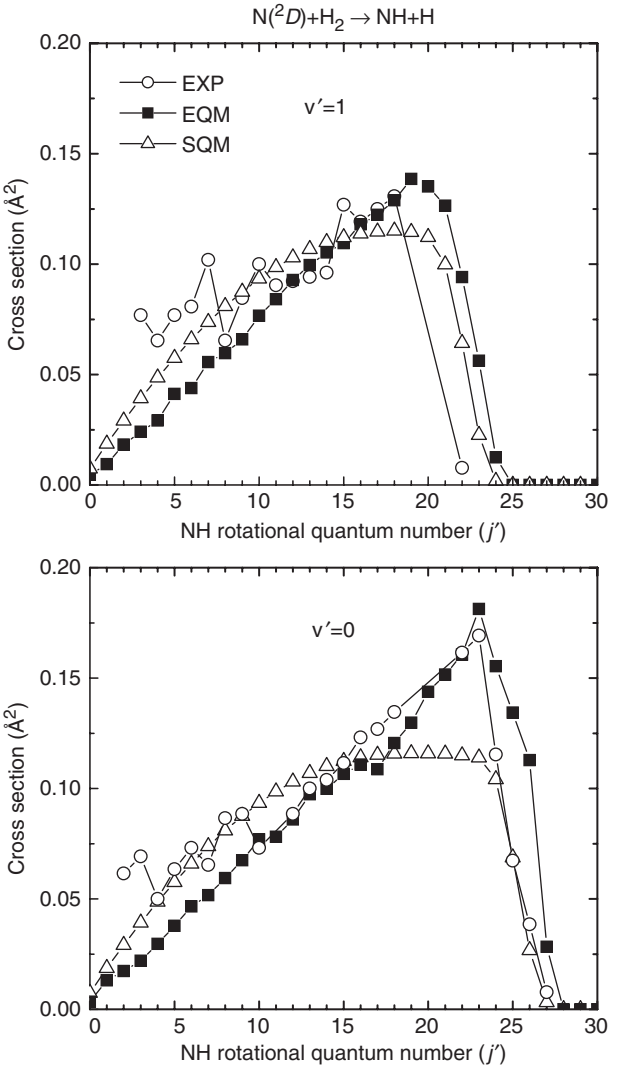

Figure 11. Rotational ICSs for the $N(^2D) + H_2(v = 0) \rightarrow NH(v', j') + H$ reaction for $v' = 0$ (top panel) and $v' = 1$ (bottom panel) at $E_c = 165$ meV. Theoretical distributions, obtained by means of an EQM calculation [135] (solid squares) and the present SQM (empty triangles), are averaged over the $j = 0$ and $j = 1$ initial rotational states to compare with the experimental results by Umemoto *et al.* [131] (empty circles).

maximum in the EQM rotational ICSs fits perfectly the experimental measurement, but the final decrease with j' exhibited by the experiment follows the statistical result, slightly colder than the exact result. The experimental $v' = 0$ distributions die around $j' = 22$ whereas both theoretical approaches extend to larger values of the final rotational excitation of the NH fragments.

Comparison between theory and experiment can be further extended to vibrational ICSs. In figure 12, EQM [135] and SQM ICSs at the same collision energy of

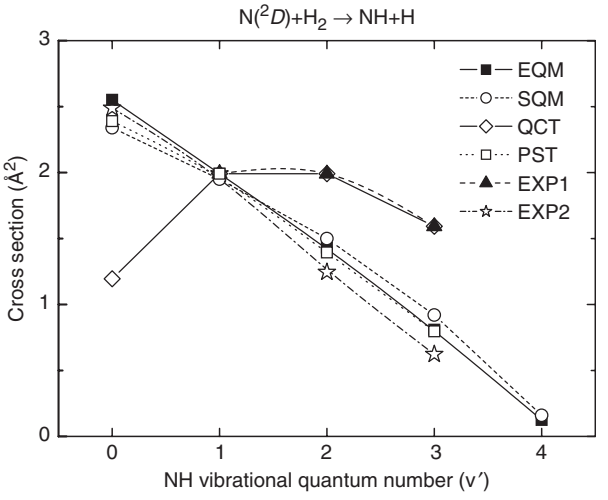

Figure 12. Final vibrational-state-selected ICSs in Å^2 for the N(^2D) + H_2($v = 0$) reaction at 165 meV collision energy. EQM results [135] are shown as solid squares and solid line; SQM results as empty circles and dashed line. Values from other theoretical calculations (QCT results from [128] are indicated with empty diamonds and solid line and values from the PST approach reported in [131] are shown in empty squares and dashed line) are also included. Comparison with experiment is established with measurements from Dodd *et al.* [126] (denoted as EXP1 with solid triangles and dashed line) and Umemoto *et al.* [136] (denoted as EXP2 with stars and dashed line). QCT and PST results, previously reported as final vibrational populations, and experimental measurements have been scaled to match the EQM prediction for the NH($j' = 1$) rotational state for the present comparison.

165 meV are compared with experimental measurements from Dodd *et al.* [126] and from the LIF study of Umemoto *et al.* [136]. Values of the vibrational distributions from previous theoretical works, the QCT calculation by Kobayashi *et al.* [128], and a PST calculation reported in [131], have been also included.

As mentioned in the introduction to section 3.2, the dynamics suggested by these two experimental investigations are completely different. Whereas the inverted vibrational distributions found in [126] are compatible with an abstraction mechanism, the decreasing populations of the product vibrational states as v' increases, reported in [136], is consistent with the statistical dynamical behaviour expected on an insertion mechanism. In fact, figure 12 reveals that experimental distribution obtained by Umemoto *et al.* is reproduced by the two statistical approaches included in the comparison, the PST of [131], and the present SQM. On the contrary, the highly inverted experimental vibration distribution of Dodd *et al.* is only reproduced by the QCT calculation of [128] which was performed on a PES where the abstraction trajectories were favoured by means of an empirical reduction of the barrier to collinear collisions. In this context the EQM results allow us to validate the statistical trend of the vibrational ICSs.

It is worth noting here that a previous comparison between theoretical and experimental vibrational distributions [136] was established considering the EQM results by Honvault and Launay [135] at a slightly lower collision energy ($E_c = 110$ meV) to reproduce the experimental conditions of 300 K [136]. One might question such a

choice for the collision energy according to the comparison between EQM and SQM rotational ICSs and the experimental distributions reported by Umemoto and collaborators for the $N + H_2$, ND_2 and $N + HD$ reactions [130–132, 136]. In these comparisons (not shown here) theoretical ICSs results are too cold to reproduce the experiment. Incidentally, the SQM approach seems to provide a better description of the exact result at 165 meV for the $N(^2D) + H_2$ reaction (see figure 1 of [19]).

The comparison between total and vibrationally resolved ICSs obtained by means of these two QM approaches at $E_c = 165$ meV for the reactant $H_2(v = 0, j = 0, 1)$ is shown in table 2. The agreement found reveals the validity of the statistical approach to describe the dynamics of the process at such a collision energy.

This aspect has been further manifested in a recent study of the process where QCT, SQM and EQM methods were compared with CMB experimental results [98]. In particular, LAB angle and TOF distributions are shown at $E_c = 165$ meV for the $N(^2D) + H_2$ reaction in comparison with the CMB findings in figures 13 and 14, respectively. Some deviations from the experiment are observed for both QM results.

Table 2. Same as table for the $N(^2D) + H_2(v=0, j=0, 1)$ collision at $E_c = 165$ meV [98].

Method	Total	$v' = 0$	$v' = 1$	$v' = 2$	$v' = 3$	$v' = 4$
EQM $j = 0$	6.68	2.48	1.91	1.40	0.79	0.10
SQM $j = 0$	6.88	2.34	1.95	1.50	0.92	0.16
EQM $j = 1$	6.69	2.41	1.83	1.43	0.86	0.15
SQM $j = 1$	6.85	2.31	1.93	1.49	0.92	0.19

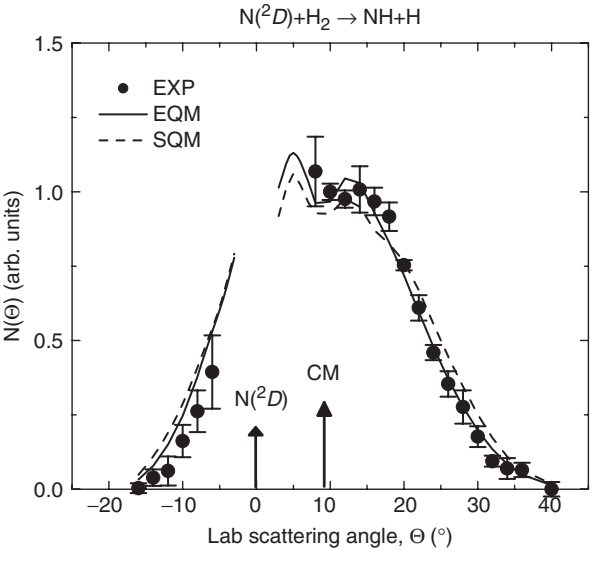

Figure 13. PLADs for the $N(^2D) + H_2$ reaction at $E_c = 165$ meV. Experimental CMB results (black points) are compared with EQM (solid line) and SQM distributions (dashed line). The figure has been adapted from [98].

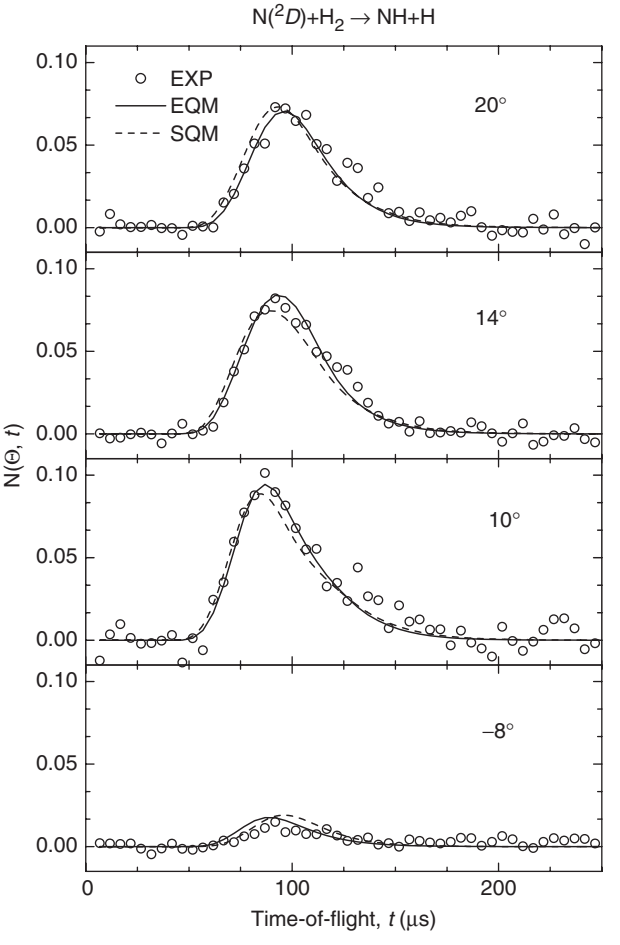

Figure 14. Comparison of the experimental CMB (empty circles), EQM (solid lines) and SQM (dashed lines) TOF distributions for the $N(^2D)+H_2$ reaction at $E_c = 165$ meV for specific values of the LAB angle: from top to bottom $\Theta = 20^\circ$, 14°, 10° and -8°. Adapted from [98].

The fit of the LAB data was found to be extremely sensitive to the fraction of energy associated with the theoretical angle-selected PLADS. Thus, although the statistical DCSs were those closer to the best-fit simulation function, the SQM results yielded an overestimation on both wings of the LAB angle distributions shown in figure 14. Slightly larger discrepancies with the CMB result were also found for the TOF distributions in comparison with the description given by the EQM results. Apart from these fine detailed aspects regarding the test with experiment, the SQM approach was conclude to provide an accurate description of QM features of the dynamics of the $N(^2D)+H_2$ collision.

An example of this is found when the theoretical DCSs for the vibrationally resolved process $N(^2D)+H_2(v=0,j=0) \rightarrow NH(v')+H$ are calculated by means of the EQM, QCT and SQM approaches. A comparison among distributions from the three

theoretical methods at 165 meV collision energy is shown in figure 15. An overall agreement is found among the different DCSs but some discrepancies are worth mentioning. The EQM DCS for the production of vibrationless NH fragments, $v' = 0$, in the top panel of figure 15 exhibits a clear preference for the backward scattering direction which neither the SQM or QCT approaches are capable of reproducing. In the particular case of the comparison with the SQM result, this discrepancy is directly connected with the result found for the rotational ICSs shown in figure 11 (see bottom panel). By examining both figures, it is easy to conclude that the peak at $\theta = 180^\circ$ is due to highly excited rotational states of the NH product fragments, since for those high j' states the statistical description was found to be lower than the exact result. For the rest of the final v' states, the SQM DCSs are in good agreement with the EQM distributions. The same is not true for the QCT results. Quasiclassical DCSs clearly fail to reproduce the EQM results for the higher product vibrational states $v' = 3$ and 4.

Finally, comparison between theory and experiment is presented for the thermal rate constants of the reactions of $N(^2D)$ with H_2 and D_2, respectively. QCT and SQM results are compared with experimental rate constants from Suzuki *et al.* [127] for both reactions in figure 16. The statistical predictions are somewhat larger than experimental measurements, specially for the $N(^2D) + H_2$ reaction. On the other hand, QCT results seem to lie too low in comparison with experiment. EQM calculations on the same PES for the $N(^2D) + H_2$ rate constant [140, 141] have confirmed that the SQM slightly overestimates the exact result, probably indicating that the lifetime of the intermediate complex formed during the course of the reaction may be shorter than assumed by the statistical approach. The method captures, however, the correct tunnelling effect in the entrance channel since the same slope of the $k(T)$ curve was found in a recent EQM calculation [141]. Results for the thermal rate constant obtained with a quantum WP method on a new PES have recently been reported [142, 143].

3.3. $O(^1D) + H_2$

The collision between an $O(^1D)$ atom and H_2 (or the corresponding isotope variants) has been the most extensively studied reaction among the $X + H_2$ collisions reviewed in section 3. Besides the interest of having the $^1A_1$ ground state of the water molecule correlated directly by the lowest PES between reactants and products, a lot of work has been done in order to elucidate the reaction mechanism of the process. Although it has been largely considered as an insertion-like benchmark reaction, an intense debate regarding the precise nature of the mechanisms which dominate the dynamics of the collision has occupied the scientific community since the early 1980s.

Early experimental investigations on the $O(^1D) + H_2$ reaction were not able to unequivocally establish the dynamical mechanisms present in the collision. Product rotational distributions for low final vibrational v' states of the fragment $OH(v', j')$ were found to exhibit a strongly marked inverted structure extending to the largest energetically accessible j' states [144–147]. Different explanations were initially given to explain these distributions (from pure insertion [144, 146, 147] to a 'microscopic branching' between insertion and abstraction [145]), but they were ultimately

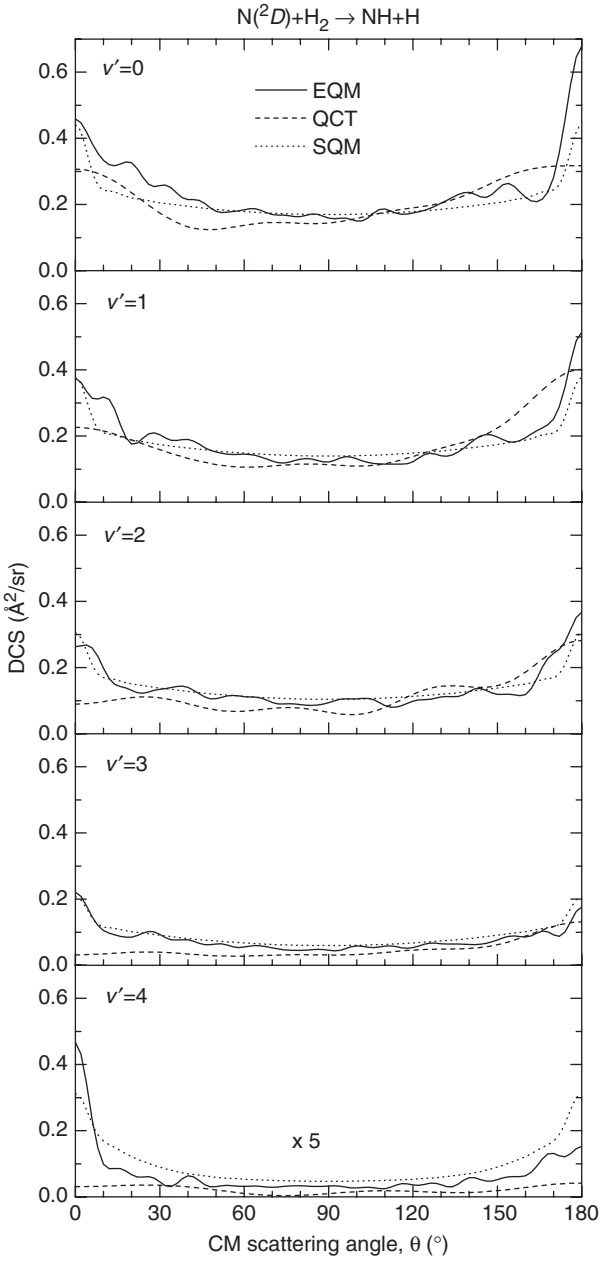

Figure 15. Theoretical DCSs for the $N(^2D) + H_2(v = 0, j = 0) \rightarrow NH(v' = 0\text{–}4) + H$ reaction at $E_c = 165$ meV. EQM results are the solid line, QCT results are the dashed line and SQM distributions are the dotted line.

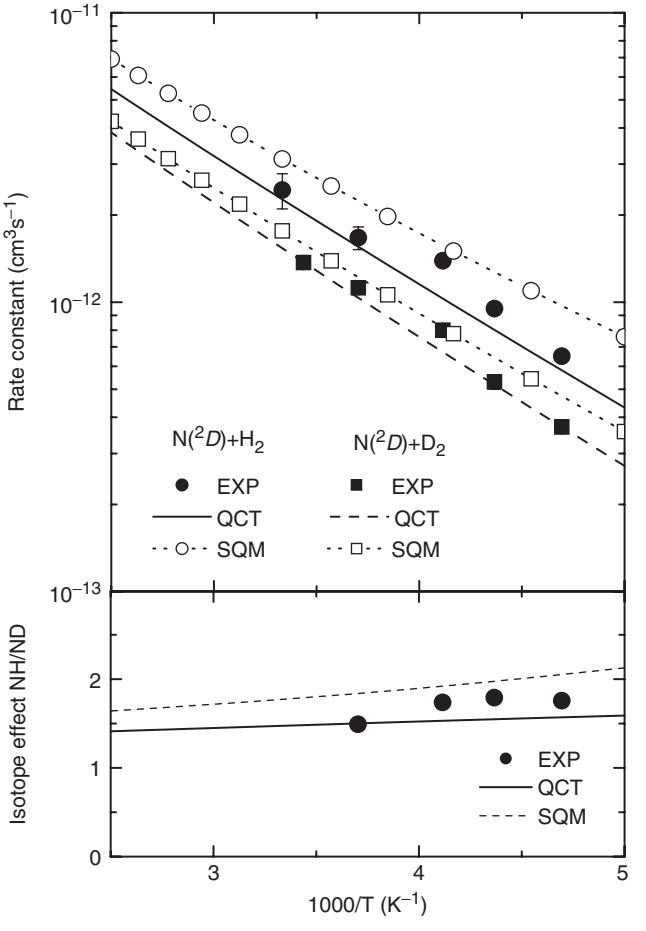

Figure 16. Thermal rate constants for the $N(^2D)+H_2$ and $N(^2D)+D_2$ reactions. QCT (solid line for $N(^2D)+H_2$ and dashed line for the $N(^2D)+D_2$ collision) and SQM (empty circles and dotted line for $N(^2D)+H_2$ and empty squares with dotted lines for $N(^2D)+D_2$) results are compared with experimental results (solid circles for $N(^2D)+H_2$ and solid squares for $N(^2D)+D_2$) [127]. The bottom panel shows the intermolecular isotope effect for reactions of $N(^2D)$ with H_2 and D_2 in terms of the temperature. In this case, experimental ratios are given as solid circles, QCT values are the solid line and SQM predictions are shown as the dashed line.

found to respond to angular momentum constraints [148]. No conclusive dynamical information could be extracted from the measured OH final vibrational distributions. They presented similarly populated low v' states ($v' = 0$–3) and a substantial decrease for the highest final vibrational state ($v' = 4$), so neither a strongly inversion with high v states favoured in comparison with the lower ones (expected in a direct abstraction mechanism) nor monotonically decreasing with v' (expected for an insertion) were found. These experimental results were mainly explained as result of an insertion mechanism [149–152], but the competition between two different dynamical reaction pathways which, respectively, excite rotation and vibration [153] and a 'direct insertion' in which the lifetime of the HOH intermediate complex was very short [154], was also

invoked. An early CMB investigation of the $O(^1D) + H_2$ reaction also concluded that essentially the oxygen atom reacts by insertion into the H_2 bond and no evidence was observed to suggest a collinear mechanism contributed significantly to the reaction [155]. Although the symmetry found in the angular distributions measured in an early CMB at 117 meV (2.7 kcal/mol) and 170 meV (4.0 kcal/mol) was interpreted as indicative of the insertion pathway, emphasis was made not to link such symmetrical features with any conclusion regarding the formation of a long-lived complex. It was related, on the contrary, to the fact that the bond rupture probability was the same for both OH bonds. This is supposed to be in fact a general result for insertion reactions involving homonuclear diatoms.

The first theoretical studies on the reaction also dealt with the issue of the identification of the mechanism which determines the dynamics of the process. Pioneering trajectory studies gave support to the insertion-like nature of the $O(^1D) + H_2$ collision [156–158]. In the studies by Schinke and Lester [156] and Whitlock *et al*. [157] product distributions obtained by the classical trajectory method were confronted by statistical predictions. In both cases, the product rotational distributions were not reproduced with a prior distribution approach. Vibrational distributions, on the other hand, did exhibit statistical behaviour at low collision energies which deviated from prior distribution predictions as E_c increases. In the calculation of [157], insertion trajectories were distinguished from those associated to direct abstraction by monitoring the minimum potential energy attained during the trajectory. The dynamical features associated to each kind of process were found to be of a very different nature. In complete contradiction with conclusions from [155], the forward–backward symmetry of the product angular distributions were interpreted as signs of an intermediate complex formation [156, 157].

Statistical approaches were of common use on the early theoretical studies on the reaction. Besides the above mentioned prior distributions tried in conjunction with trajectory calculations [156, 157], different statistical approaches were employed to compare experimental findings. Thus, PST predictions were compared with QCT results and LIF measurements of rotational product distributions [144]. Important deviations of the experimental result from the statistical predictions were observed. Surprisal analysis was used to estimate the product branching ratio of the $O(^1D) + HD$ reaction [147]. A statistically based information theory approach and a PST calculation were employed as theoretical counterparts of the LIF product distributions reported in [145]. The report of the CMB results from [155] included a PST prediction for the product energy distribution which was found to provide fair qualitative agreement with the experimental measurements. A statistical algorithm [148, 159] yielded good accord with both OH product rotational distributions from LIF measurements [144] and LAB angular distributions from the CMB investigation by Buss *et al*. [155]. Microcanonical statistical theory and PST results were used to compare with QCT estimations of both vibrational product distributions and average product rotational energy on the collision of $O(^1D)$ with H_2, D_2, and HD [160]. Whereas the PST approach yielded results in good accord with the distributions from the trajectory calculation on the $O(^1D) + H_2$ reaction, significant deviations from statistical behaviour were noticed for the OD distributions on the O + HD process.

More recently, a generalized version of the present SQM was employed to study the $O(^1D) + H_2 \rightarrow OH(^2\Pi) + H$ reaction [108]. This extended model was designed to include the electronic and spin–orbit effects among all PESs which correlate with the product fragments. A strong propensity for the production of the $\Pi(A')$, Λ-doublet states of the OH species was found, thus confirming previous experimental results. Moreover non-statistical population of the OH Λ-doublet levels was interpreted as a consequence of the bond breaking in the intermediate complex H_2O. A similar investigation of $D(^2S) + OH(^2\Pi) \rightarrow OD + H(^2S)$ found a negative temperature dependence and a preference for the formation of OD (A') , Λ-doublet level [109].

One of the most commonly studied indicators to probe the dynamics of the isotope variant reaction $O(^1D) + HD$ is the isotopic branching ratio H/D between either the two different product channels $OD + H$ and $OH + D$, respectively, or the $O + H_2$ and $O + D_2$ processes. A general result establishes that abstraction processes are accompanied by a value of lower than one for such a ratio while insertion processes would produce a ratio greater than one [164]. With the only exception of a statistical value of 0.08 reported as a private communication [67], the H/D ratio has been systematically found in both experimental [147, 161–164] and theoretical [160, 165] investigations larger than unity with values which range from 1.04 [160] to 2.6 [165].

In all this abstraction versus insertion controversy little attention was given to the possible existence of contributions from excited PESs influencing the dynamics of the reaction between $O(^1D)$ and H_2 or HD. The QCT calculation by Berg *et al.* [166] was the only reference in the literature from the early 1990s in which both of the energetically accessible PESs of the system were included. The authors found that trajectories which sample the excited PES yield different dynamics from those which remain on the ground PES. Renewed interest in this reaction has been motivated by the recent experimental findings of Liu and collaborators (see [6] for a review) where the participation of abstraction was clearly manifested. A CMB investigation of the $O(^1D) + HD$ reaction found forward–backward asymmetry features on the angular distributions besides a substantially larger translational energy release on the $O + HD$ channel in comparison with the $OH + D$ one [167]. The peculiar energy dependence found for the ICSs, which decrease rapidly up to near 87 meV (2 kcal/mol) to experiment a gradual increase beyond that energy, was interpreted as the interplay of two reaction mechanisms [168]. In addition the ratio H/D remains constant at low energies and starts increasing linearly once this value of 87 meV for the collision energy is reached. An estimation of the microscopic branching between the two reaction mechanisms was given. The dramatic variation on both the angular distributions and angle-specific PTE distributions with a slight change in the total available energy were also attributed to the onset of an abstraction reaction pathway [169, 170]. Besides all these experimental studies, the development of *ab initio* excited PESs [171] allowed workers to complete the overall dynamical picture for this reactive process: whereas it was generally accepted that the reaction on the ground $1A'$ PES proceeds via an insertion mechanism [163, 172–174], dynamics on excited PESs $(1A'', 2A', \ldots)$ is the result on an abstraction reaction pathway [167–171]. These conclusions were nevertheless partially questioned in successive studies of the $O(^1D) + HD$ reaction regarding the possible participation of excited PESs. In these works, QCT calculations reproduced different experimental findings for the $OH + D$ channel based solely on the

ground PES [175–178], although evidence of contributions from the $1A''$ PES were found for the OD + H exit channel at the collision energy of 196 meV [177]. This issue is far from being completely understood simply in terms of different reaction mechanisms restricted to different energy regimes, since findings of the excited $1A''$ PES participation for the OH + D product channel at a collision energy of 100 meV [179] contrast with their apparent lack of importance at a higher value of $E_c = 196$ meV [177].

Experimental investigation of the state-to-state dynamics of the reaction has been possible by means of the high-resolution H atom Rydberg 'tagging' TOF technique (see [180] for a review of this work). For the $O(^1D) + H_2$ collision, the total reaction product DCS was found to be roughly forward–backward symmetric at 56 meV (1.7 kcal/mol) [181] although vibrationally resolved OH(v') products exhibited different angular distributions according to the different final vibrational excitation v'. The authors concluded that, at that collision energy, the dynamics of the reaction could be described as an insertion mechanism with small contribution from the collinear abstraction pathway. A recent comparison with QCT and EQM results [178] showed that the quantum results exhibited large peaks in the forward–backward scattering directions which were not present in the experimental measurements. Passage from the former at 56 meV to the latter mechanism when the energy is increased up to 139 meV (3.2 kcal/mmol) was observed for the $O(^1D) + D_2$ reaction by analysis of the OD product distributions [182]. The experimental findings on the $O(^1D) + HD$ reaction [183] revealed some asymmetry on the angular OD product distributions, which were interpreted as examples of non-symmetric features on an insertion process.

In a recent comparison between a time-dependent (TD) WP calculation and Rydberg H-atom TOF spectroscopic measurements on the $O(^1D) + HD \rightarrow OH + D$ reaction [184] it was found that the ground PES was sufficient to describe the dynamics of the process and non-adiabatic effects involving the electronic excited pathway are in principle small. The overall forward–backward product scattering symmetry was interpreted as the result of a long-lived complex-formation reaction.

The statistical calculations were performed on the ground $1A'$ PES by Dobbyn and Knowles [185, 186].

In figure 17 the probabilities of the $O(^1D) + H_2(v = 0, j = 0)$ reaction for $J = 0$ are shown up to a collision energy of 0.5 eV. Statistical total and final vibrational state resolved reaction probabilities are compared with results from EQM calculations by the TI method of Launay and Honvault. As in the previous cases (especially for $C(^1D) + H_2$ in figure 2) the statistical capture theory predicts a larger reactivity than the exact method, although the overestimation of the total probability at low energies seems not to come from the formation of a specific vibrational state v' of the OH product fragments. A clear discrepancy, however, is found for the highest final vibrational state considered in this energy range ($v' = 5$ in the bottom right panel), which is the only case exhibiting a reaction threshold.

The SQM reaction probability in terms of the total angular momentum or opacity function at 56 meV collision energy is compared with the EQM results of Honvault and Launay in figure 18. Both total and final vibrational state resolved statistical opacity functions reproduce the EQM result fairly well. The EQM calculations, also performed solely on the ground $1A'$ PES, seem therefore to be describing an insertion process for the reaction at this energy regime.

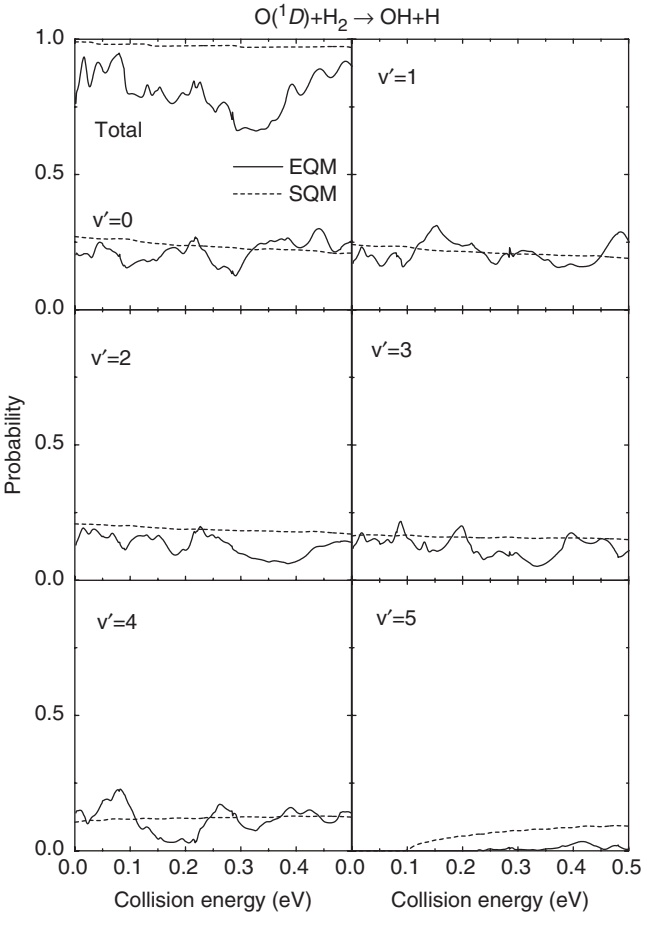

Figure 17. Total and vibrationally resolved reaction probability for $O(^1D) + H_2(v = 0, j = 0)$ reaction probability for a zero total angular momentum. SQM results (dashed line) are compared with EQM probabilities (solid line) from the calculations of Honvault and Launay. Total and final-state-selected $OH(v' = 0)$ probabilities are shown in the top left panel. Probabilities for formation of $OH(v' = 1–5)$ products are presented separately in the rest of the panels.

SQM predictions are compared here with results from EQM calculations [178, 187] and experimental measurements by the H-atom Rydberg 'tagging' TOF technique [178, 181]. In figure 19 state-to-state ICSs for the $O(^1D) + H_2(v = 0, j = 0) \rightarrow OH(v', j') + H$ reaction at 56 meV collision energy displayed for each v' state are shown. In particular, the comparison between the SQM and the EQM approaches reveals that rotational distributions behave statistically for almost all the product vibrational states. The typical appearance of these ICSs increases monotonically with the final rotational quantum state j', reaching a maximum at one of the higher states energetically accessible. The only significant discrepancies appear for the final vibrational ground state $v' = 0$ and first excited $v' = 1$ (in the top and second panel, respectively, of figure 19), for which the statistical predictions exceed the exact result up to

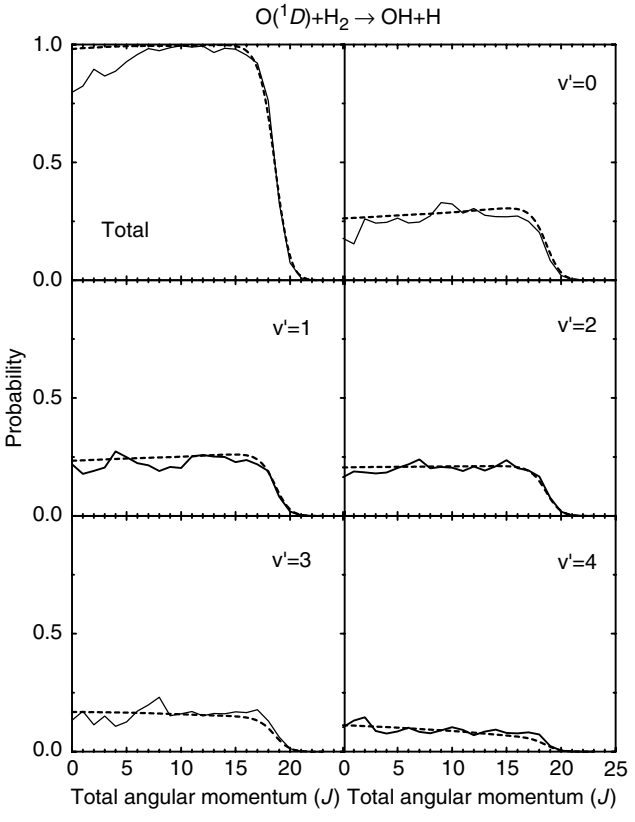

Figure 18. Opacity functions for the $O(^1D) + H_2(v = 0, j = 0)$ reaction at 56 meV collision energy. EQM results (solid line) from Honvault and Launay are compared with statistical predictions (dashed line) for the total reaction probability (top panel) and for the final vibrational state $v' = 0$–4 in the rest of the panels.

around $j' = 18, 19$ and decay faster to yield slightly colder distributions than the EQM cross-sections. The accord, however, for the rest of the final vibrational excitations shown in figure 19 is excellent. The description of the experimentally deduced ICSs by means of the statistical method is not as good until the vibrational $v' = 3$ state. Up to then, the experimental distributions display a broader maximum which involve several final rotational states displaying a structure that even the EQM method has some difficulties in reproducing. Incidentally, both theoretical methods seem to overestimate experiment for the $v' = 4$ (in the bottom panel). Interest in finding such good agreement in this comparison with both the EQM and experimental results relies on the conclusions reported in [178] which stated that neglecting the collinear abstraction contribution from the excited $1A''$ PES has no consequences in the comparison with experimental measurements. Reproduction of the main dynamical features of the process by means of statistical calculations performed on the ground electronic state remarks the insertion-like character of the reaction at this collision energy.

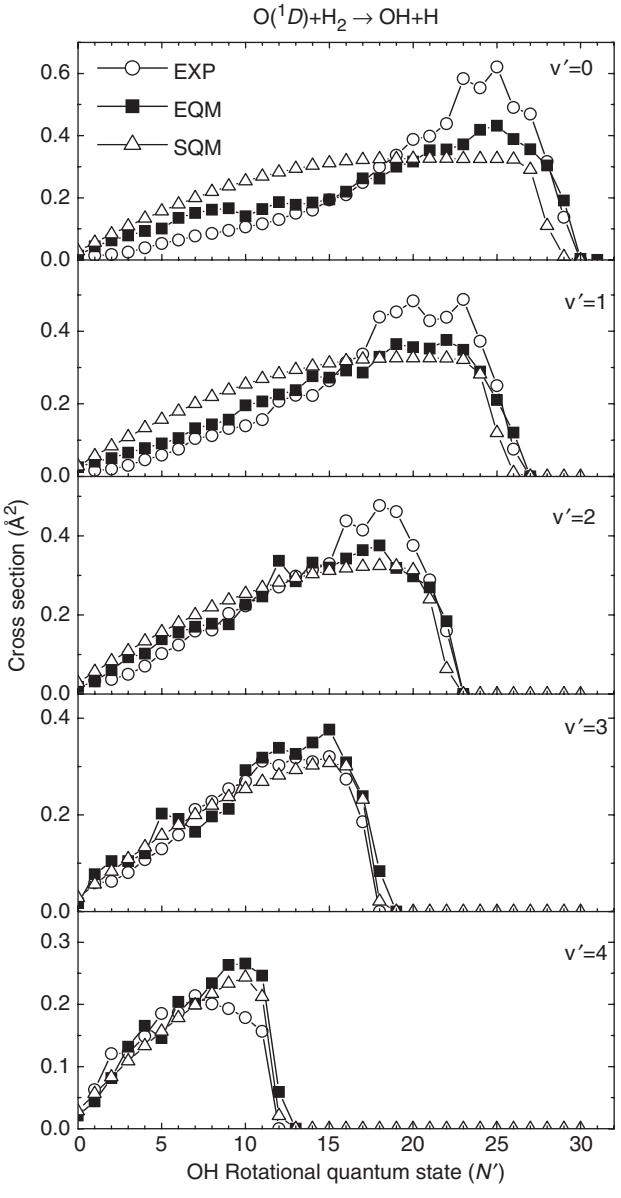

Figure 19. State-to-state ICSs for $O(^1D) + H_2(v = 0, j = 0) \rightarrow OH(v', j') + H$ reaction at 56 meV collision energy. $v' = 0$–4 final vibrational state resolved cross-sections are shown in the panels from top to bottom. SQM results (empty triangles with thin solid lines) are compared with experimental H atom Rydberg 'tagging' TOF measurements (empty circles with solid lines) [178, 181] and EQM results (black squares and solid lines) [178, 187].

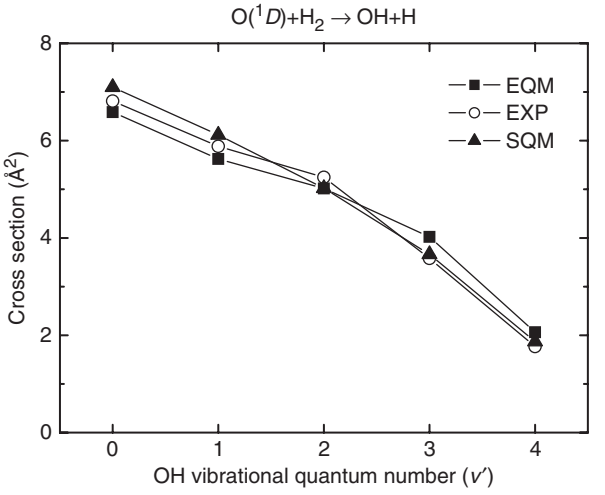

Figure 20. Final vibrational state resolved ICSs for the $O(^1D) + H_2(v = 0, j = 0) \rightarrow OH(v') + H$ reaction at 56 meV collision energy. As in figure 19, EQM results [178, 187] and experimental measurements [178, 181] are compared with the SQM cross-sections.

Table 3. EQM [178] and SQM ICSs for the $O(^1D)+H_2(v = 0, j = 0)$ reaction at $E_c = 56$ meV. Units are Å^2.

Method	Total	$v' = 0$	$v' = 1$	$v' = 2$	$v' = 3$	$v' = 4$
EQM $j = 0$	23.31	6.58	5.62	5.01	4.02	2.06
SQM $j = 0$	23.77	7.10	6.12	5.02	3.66	1.87

Vibrationally resolved ICSs obtained summing over all final rotational j' states for each vibrational state v' at $E_c = 56$ meV are shown in figure 20 and in table 3. Comparison with the EQM cross-sections, also included in the figure, shows that the statistical distributions remain larger than the exact result for the lower vibrational states ($v' < 2$), thus indicating that, for those v' states, contributions from the lower rotational j' states, for which the SQM predicts a larger reactivity than the EQM calculation, largely compensate the underestimation found at the higher rotational states (see figure 19). Beyond $v' = 2$, differences between both theoretical calculations are not significant as indicated by the value for the total ICS shown in table 3 predicted by both methods. The experimentally measured distributions from [178, 181], on the other hand, lie between theoretical predictions from the EQM and SQM approaches for $v' < 2$, but are fairly well reproduced by the statistical values at the higher final vibrational excitations. This agreement clearly supports the statistical nature of the collision for this low-energy regime.

In figure 21, the SQM DCS at 56 meV for both the total reaction and those processes for which the final vibrational state is selected are compared with EQM results [178, 187]. The comparison is also extended to experimental results by Yang and collaborators [178, 187]. One of the most relevant things from such a comparison between theory and experiment is that theoretical angular distributions exhibit a much more

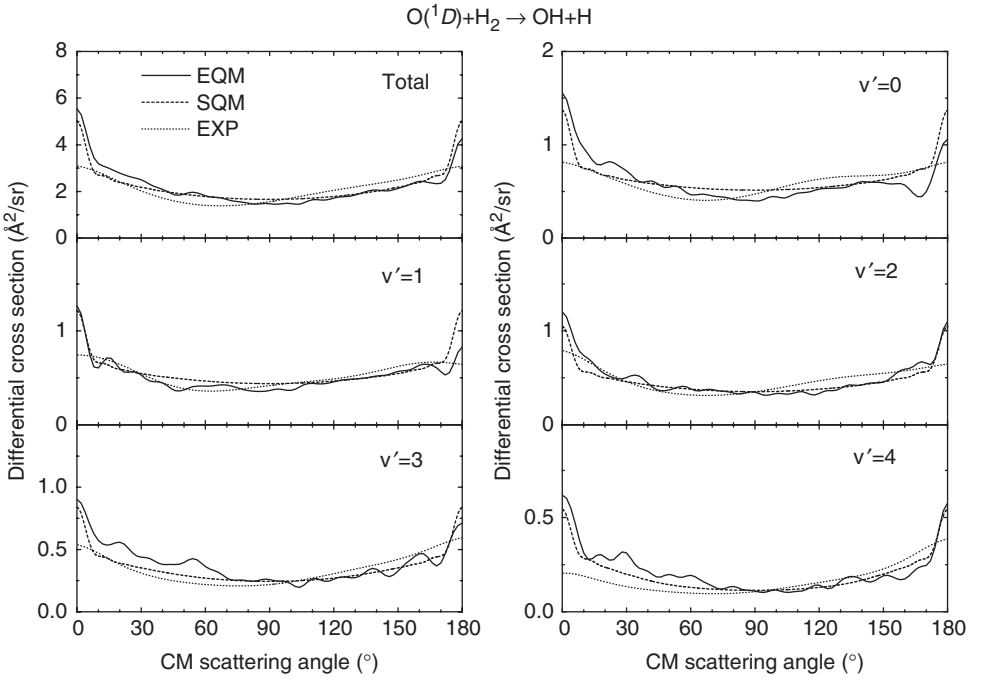

Figure 21. DCSs for the total (left top panel) and vibrationally resolved reaction from $O(^1D) + H_2(v = 0, j = 0)$ reactants at 56 meV collision energy. EQM results from [178, 181] are shown as the solid line, experiment [178, 181] is shown as the dotted line and SQM results are the dashed line.

marked forward–backward peaked structure than the measured DCSs. This was previously reported in [178], where interestingly a QCT calculation (not shown here) was found to provide a better description of the much flatter experimental distributions in the 0° and 180° scattering directions. In addition, experiment finds in all cases, both total reaction and vibrationally resolved collisions, a more forward–backward symmetrical character in the DCSs than the EQM result.

The comparison between the EQM and SQM angular distributions reveals that fairly good agreement is found between both quantum approaches for the DCSs shown in figure 21 at the collision energy under consideration. The statistical prediction gives a good overall description of the exact results, yielding the right behaviour at the sideways direction and reproducing correctly at least one of the peaks in either the forward or backward directions when some asymmetry is found in the EQM distribution. Despite the state-to-state EQM DCSs being in general highly symmetric, a slight propensity to the forward direction is detected for the total reaction DCS. That seems to come from contributions of collisions ending in specific final vibrational states, such as $v' = 0$, which systematically produces forward-preferred angular distributions. It is difficult to extract definitive conclusions regarding a possible evolution of the angular behaviour as the collision energy increases from a comparison (not shown here) between EQM and SQM DCSs at 25 meV, 56 meV and 100 meV. Apart from the already mentioned [187] similarities found between the cases at 56

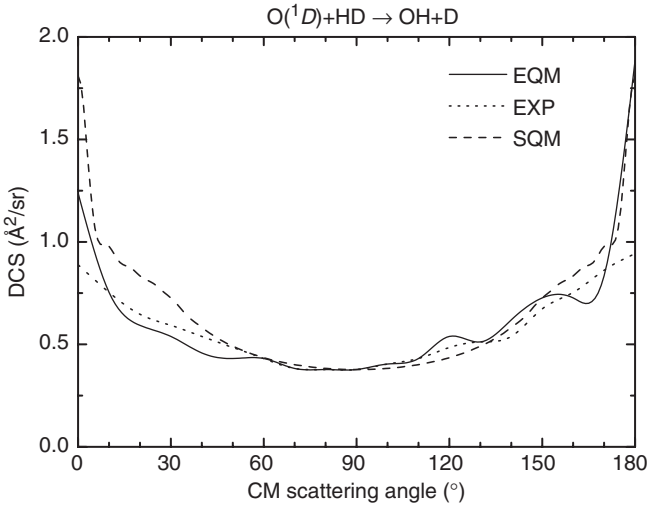

Figure 22. DCSs for the $O(^1D) + HD(v = 0, j = 0) \rightarrow OH + D$ reaction at the 74 meV collision energy. The SQM distribution (dashed line) is compared with Rydberg H-atom TOF spectroscopic measurements [184] (dotted line) and a TD WP EQM calculation (solid line) [184].

and 100 meV in comparison with the DCS at 25 meV and the appearance of an almost isotropic distribution for the $O(^1D) + H_2(v = 0, j = 0) \rightarrow OH(v' = 3) + H$ reaction at the lower energy out the three mentioned, no remarkable effects are noticed. Moreover, the agreement between the statistical and the exact results seem not to change appreciably with the energy. It might be mentioned that while a slight deviation from the statistical prediction for the forward peak with respect to the EQM result is noticed the opposite is found for the backward maximum. Those effects, however, are too small to conclude something definitive from them.

The SQM approach was also applied to the $O(^1D) + HD \rightarrow OH + D$ reaction and results have been compared with those recently reported in the experimental and theoretical study on this reaction [184]. In figure 22 DCSs at the collision energy of 74 meV are shown. The statistical distribution is compared with the TD WP calculations and the Rydberg H-atom TOF measurements of [184]. Both TD WP and experimental DCSs have been scaled to agree with the statistical prediction for the sideways scattering. The interesting result is that this choice also brings the TD WP cross-section into perfect agreement in the backwards direction with the SQM result. Despite the forward–backward symmetry exhibited by the experimental result the statistical DCS describes much better the EQM calculation with the exception of the forward scattering peak predicted in the TD WP angular distribution.

3.4. $S(^1D) + H_2$

The literature on the $S(^1D) + H_2$ reaction is probably much smaller than on some of the others $X + H_2$ collisions reviewed in section 3.

The extensive CMB study on this process and its isotope variants by Lee and Liu has supplied strong evidence to invoke an insertion mechanism to describe the dynamics of this reaction at low collisional energy [188–190]. The lack of a gradual raise with the collision energy of the excitation functions [188], the complete independence of the ratio between the production of SD + H versus SH + D for the $S(^1D) + HD$ collision [188] and the forward–backward symmetry found for the $S(^1D) + H_2$ [190] and the $S(^1D) + D_2$ [189] DCSs were interpreted as indications of a complex-forming reaction pathway.

Several intriguing questions were nevertheless raised by this experimental investigation. Thus the unusual trend followed by the ICSs corresponding to the collision of the S atom with H_2, D_2 or HD, forced the CMB thermal rate constants to follow the sequence $k_{HD} > k_{H_2} \approx k_{D_2}$, in comparison with the prediction of $k_{H_2} > k_{HD} > k_{D_2}$ from a simple state theory. The experimental value for the isotope ratio mentioned above was found to be about 0.7, which would not be consistent with an insertion mechanism according with the classification which would associate the H/D ratio lower than 1 for direct abstraction reactions and values larger than 1 for insertion processes [164]. In addition, deviations from the symmetrical appearance of the DCS when the collisional energy increases and bimodal rotational distributions for the $S(^1D) + H_2$ reaction [190] also raise some questions about the precise nature of the dynamics of the processes.

Interestingly, QCT and statistical approaches have failed to completely reproduce some of these CMB findings. QCT calculations on an *ab initio* PES which does not permit abstraction [191, 192] did not predict any isotope effects in clear opposition with the experimental result. Moreover significant quantitative discrepancies were found between the QCT and CMB PTE distributions. Improvements on the PES did not cause relevant changes in the observed dynamics with the QCT calculation [193]. Comparison of results from a different QCT study on the $S(^1D) + H_2$ reaction with experimental measurements at $E_c = 0.171$ eV (3.96 kcal/mol) also revealed serious discrepancies [194].

Regarding the attempts to study the reaction on statistical grounds, we should mention here the reasonably good description given by a PST approach of the forward–backward scattering direction of the experimental PTE distributions for the $S(^1D) + D_2$ at $E_c = 0.23$ eV (5.3 kcal/mol). It clearly failed, nevertheless, to describe the sideward direction on the product state distributions and the forward–backward DCS measured in experiment [189]. A collision complex model [195] did not reproduce either the order of the ICSs for all the isotope collisions with $S(^1D)$ or the drop of their value with increasing energy. In a more recent study, the WP approach of the present SQM was applied to the reaction of $S(^1D)$ with H_2, HD and D_2 [106]. This work also found some of the previously mentioned inconsistencies between theory and experiment such as the lack of a theoretical prediction for the CMB isotope effect and a different energy dependence of the calculated and measured σ_{SD}/σ_{SH} branching ratio for the $S(^1D) + HD$ collision.

The only existing EQM calculation to date on the $S(^1D) + H_2$ reaction has been performed at $E_c = 97$ meV (2.24 kcal/mol) [194, 196]. The agreement found with experimental DCSs and PTE distributions at that specific collision energy was extremely good

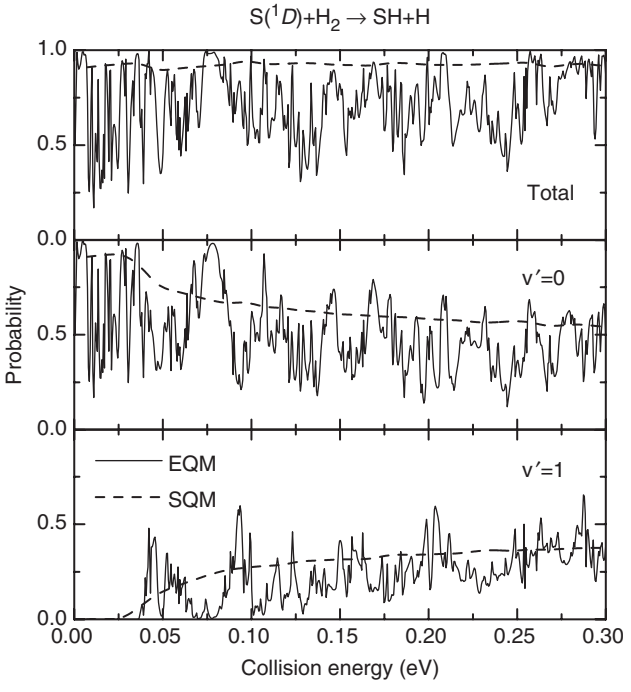

Figure 23. Total and vibrationally resolved reaction probabilities for $S(^1D) + H_2(v = 0, j = 0)$ for a zero total angular momentum, $J = 0$, up to a 0.3 eV collision energy. EQM results [197] (solid line) are compared with statistical predictions (dashed line) for the total reaction (top panel) and the state-to-state selected processes of formation of $SH(v' = 0)$ (middle panel) and $SH(v' = 1)$ (bottom panel) product fragments.

[196], although opposite conclusions regarding the disposal of vibrational excitation in the products were obtained [194].

The statistical calculations presented here have been carried out on the PES by Ho *et al*. [193].

In figure 23 the $J = 0$ reaction probabilities for the $S(^1D) + H_2$ collision are shown in comparison with results from an EQM calculation [197]. The total reaction probability in the top panel of the figure shows that the statistical capture theory approach slightly overestimates the exact probability. The reproduction of the vibrationally resolved probabilities for the ground $v' = 0$ and first excited $v' = 1$ vibrational state of the SH product fragment is fairly good. The average description turns out to be somewhat larger than the EQM probabilities but describes correctly the existing threshold for the formation of $SH(v' = 1)$ and follows the right trend of the two EQM final-state-selected reaction probabilities in the energy regime considered.

As in the cases of the previous $X + H_2$ reactions included in this review, the comparison with an EQM result for the opacity functions turns out to be quite good. Such a comparison at a 97 meV collision energy (not shown here, see figure 3 of [20]) with the TI calculation by Honvault and Launay predicts a good performance of the SQM to reproduce averaged quantities. The first example reviewed here is the rotational

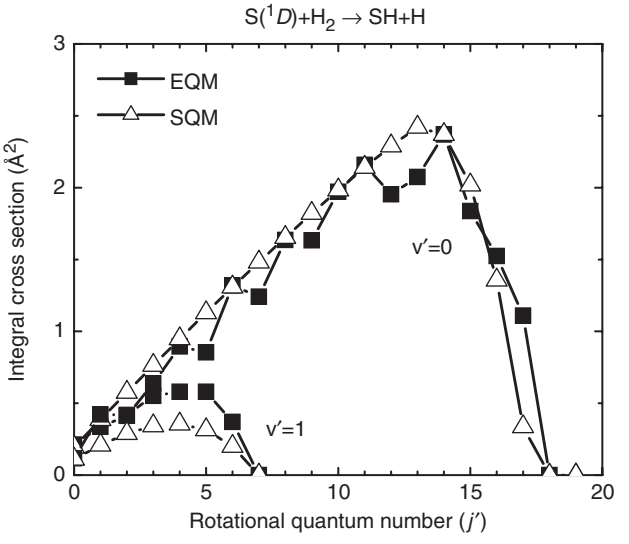

Figure 24. ICSs for the state-to-state $S(^1D) + H_2(v = 0, j = 0) \rightarrow SH(v', j') + H$ reaction at 97 meV collision energy for $v' = 0$ and 1. EQM distributions [194] (black squares and lines) are compared with the SQM results (empty triangles).

Table 4. EQM total σ and vibrationally resolved $\sigma_{v'}$ ICSs for the $S(^1D) + H_2(v = 0, j = 0,1)$ reaction at a collision energy of $E_c = 97$ meV. EQM results have been taken from [194]. Cross-sections are given in Å^2.

Method	Total	$v' = 0$	$v' = 1$
EQM $j = 0$	27.21	24.17	3.04
SQM $j = 0$	27.00	25.18	1.82
EQM $j = 1$	27.42	23.63	3.79
SQM $j = 1$	27.89	25.44	2.45

ICSs at that specific collision energy for the reactions from $H_2(v = 0, j = 0)$ to the final vibrational states $v' = 0$ and 1 of SH shown in figure 24. The comparison between the SQM and the EQM calculation of [194], incidentally slightly better than that previously reported in [106], shows the statistical nature of the rotational distributions at this collision energy. Moreover it is worth mentioning that the agreement found with the exact calculation improves that found for the $N(^2D) + H_2$ and $O(^1D) + H_2$ reactions shown in figures 11 and 19, respectively.

A further indication of the accurate description yielded by the SQM on the dynamics of the $S(^1D) + H_2$ reaction is shown in table 4, where values for both the total and vibrationally resolved ICSs are shown comparatively with EQM results from [123]. The good accord expected for the case of the reaction initiated from the rotationless H_2 species in view of the state-to-state cross-sections presented in figure 24 is also accompanied by a close agreement for the case of collisions with the H_2 rotationally excited to $j = 1$.

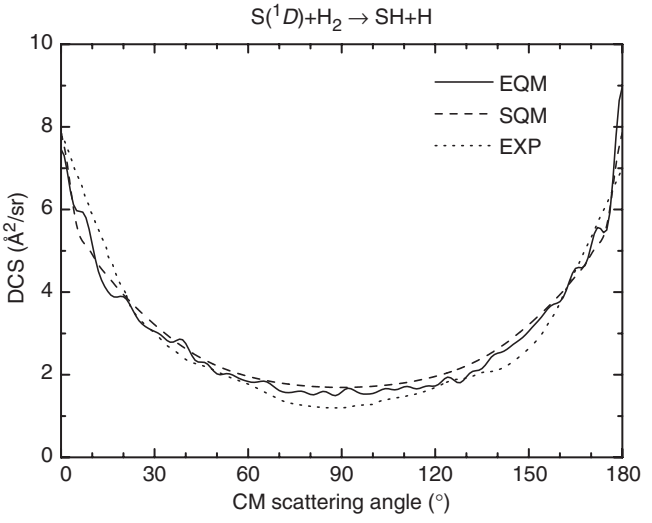

Figure 25. DCSs for the $S(^1D) + H_2$ reaction at $E_c = 97$ meV. Theoretical results, averaged on the two $H_2(v = 0, j = 0)$ and $H_2(v = 0, j = 1)$ initial states obtained by means of an EQM calculation [196] (solid line) and the SQM (dashed line) are compared with the experimental result by Lee and Liu [190].

A similar good accord is found between the SQM and EQM [196] DCSs at the same collision energy of 97 meV as shown in figure 25. Despite the slight asymmetry of the exact angular distribution favouring backward scattering, the overall description yielded by the statistical approach is remarkable. Also included in the same figure, the CMB experimentally deduced DCS by Lee and Liu [190] has been scaled to bring it in comparison with the EQM and SQM predictions. The theoretical distributions, on the other hand, have been obtained after averaging between the ground and first excited initial rotational states of the vibrationless $H_2(v = 0)$ reactant fragment. The intrinsic forward–backward symmetrical appearance of the experimental results, previously attributed as characteristic of a complex-forming reaction [190], shows the precise agreement with the statistical distribution. As shown before [106] the departure of such symmetry of the experimental measurements at higher collision energies [190] also involves a deviation from the statistical behaviour.

A nice test involving comparison with both EQM results and experiment is provided by the PTE distribution. In figure 26, such distributions for the $S(^1D) + H_2$ reaction at $E_c = 97$ meV are compared. The total reaction probabilities obtained by means of the EQM and SQM approaches after a similar initial rotational state average as in the case of the DCSs are compared with the measurements of [190]. Theoretical final vibrational state selected distributions for production of $SH(v' = 0)$ and $SH(v' = 1)$ are also included in the figure. Although the experimental result presents a less structured profile, both theoretical distributions give a fairly good description of the CMB measurement. In particular theory gives an account of the origin of the peak at low PTE, attributed to the final ground state $v' = 0$. The EQM and SQM results differ somewhat at the maximum of the PTE distribution due to the $v' = 1$ contribution.

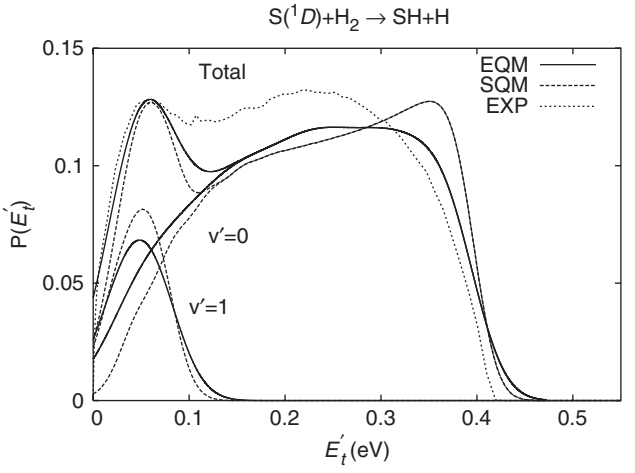

Figure 26. PTE distribution at 97 meV collision energy for the $S(^1D) + H_2$ reaction. EQM results (solid line) from [196] and the SQM distributions (dashed line) for the total reaction process are compared with the experimentally obtained result of [190] (dotted line). Comparison between results for the final vibrational v' state selected reactions obtained with both theoretical methods is also included.

In connection with the above mentioned possible transition from a complex-forming reaction mechanism at low collision energies to the non-statistical dynamics at higher energies suggested by the experimental work on $S(^1D) + H_2$ [190], it is interesting to analyse the results of a similar CMB investigation on the isotope variant process $S(^1D) + D_2$ [189]. Despite the high value of the collision energy ($E_c = 230$ meV) considered in this study, clear evidence of forward–backward symmetry was found for product angular and PTE distributions. The analysis given in [189] by means of a PST approach did not yield a good description of the experimental results. Here results obtained with the SQM are compared with some of the results of that CMB study. In figure 27, the statistical DCS at 230 meV collision energy is presented in comparison with the experimental distribution [189]. As in the previous comparisons with experiment, the theoretical DCS has been averaged over the $D_2(v = 0, j = 0)$ and $D_2(v = 0, j = 1)$ initial states and the measured distribution has been scaled to agree with the forward scattering peak of the statistical prediction. The good accord found between both distributions, consistent with results recently reported in [106], invites us to consider the highly statistical nature of the process at this collision energy in clear contradiction with the more isotropic prediction given by the PST approach employed in [189].

The comparison between the experimental PTE distribution [189] at the same collision energy and its statistical correspondence for the $S(^1D) + D_2$ reaction is shown in figure 28. The experimental result, scaled to compare with the theoretical one, has a similar broad profile to the distribution for the $S(^1D) + H_2$ reaction shown in figure 28, in which some indications of an underlying structure of maximum peaks seem to be suggested. The SQM distribution, on the other hand, exhibits more clearly

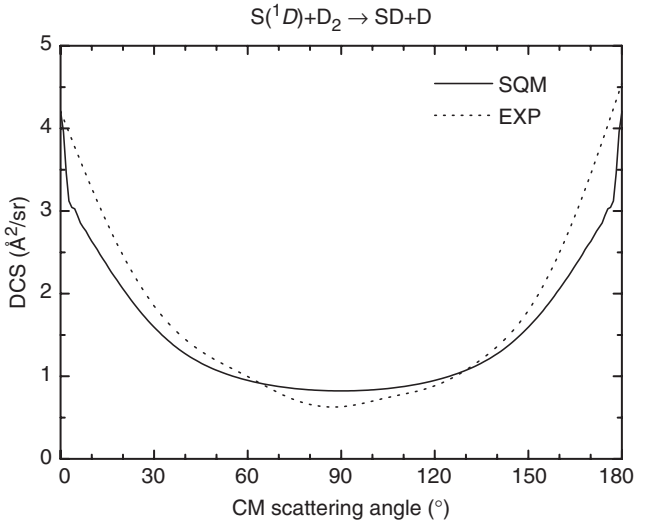

Figure 27. DCSs for the $S(^1D) + D_2$ reaction at 230 meV collision energy. The SQM result (solid line) averaged for the $D_2(v = 0, j = 0)$ and $D_2(v = 0, j = 1)$ initial states are compared with the CMB experimental distribution (dotted line) obtained by Lee and Liu. Experimental DCS has been adapted from [189].

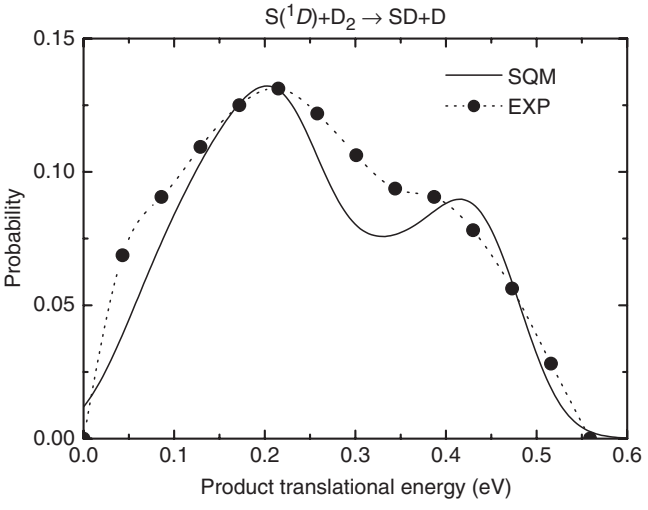

Figure 28. PTE distribution for the $S(^1D) + D_2$ reaction at 230 meV collision energy. Comparison between the initial rotational state averaged result (solid line) and the experimental measurement (black circles and dotted line) adapted from [189] is shown.

those maxima and in particular the structures centred around 0.2 eV and 0.4 eV seem to correspond to the global maximum and a shoulder feature, respectively. In general, from figure 28 quite decent agreement may be concluded between the statistical and experimental PTE distributions.

4. The $H^+ + H_2$ reaction: an ion–diatom insertion process

One of the topological features on the PES associated to the $H^+ + H_2$ reaction, which has attracted more attention, is the crossing between the energy curves of the states which correlate to $H^+ + H_2$ and $H_2^+ + H$ at about 1.6 eV above the H_2 well minimum at the asymptote. This electronic curve-crossing has meant that much of the interest on the study of this collision has been devoted to the determination, for energies beyond that point, of the competition among the three different existing reaction pathways, that is:

(i) the reactive charge transfer, in which the charge ends in the new diatom formed in the process;
(ii) the non-reactive charge transfer channel, in which the process merely supposes the charge migration from the ion to the diatom; and
(iii) the reactive non-charge transfer channel, in which the charge remains in the product monatomic ion.

For the low-energy regime below the electronic curve-crossing, however, no attention to non-adiabatic effects and contributions from triplet states is required. The goal of the studies included in the present work is the study solely of the case (iii) exchange processes mentioned above.

The existence of a deep potential well for the collision $H^+ + H_2$ (about 4.3 eV) and the lack of any barrier at the entrance channel invite us to think that the reaction proceeds via an insertion mechanism. In fact, on previous studies on different isotope arrangements of the H_3^+ system [198–201] it was concluded that the dynamics of these processes evolve from a short-lived collision intermediate mechanism below about 3 eV to a predominantly direct impulsive reaction pathway at larger energies ($E_c > 4.5$ eV). Complex-formation cross-sections for the $D^+ + D_2$, $D^+ + H_2$, and $H^+ + D_2$ reactions [201] were found to decrease rapidly as the collision energy increases. In addition, lifetimes of these intermediate complexes also shortened when the collision energy was augmented [200]. Analysis of experimental energy distributions of reactant and product ions on the atomic–ion exchange reactions $D^+ + H_2 \rightarrow HD + H^+$, $H^+ + D_2 \rightarrow HD + D^+$, and $D^+ + HD \rightarrow D_2 + H^+$, indicated a complex-forming mechanism at low collision energies and a direct reaction at higher energies [202]. However, the authors of that experimental study considered that a description of the dynamics of these reactions simply in terms of 'complex formation' versus 'direct reaction' was an oversimplification of the question. Although the same insertion-to-abstraction mechanism transition with increasing energy should be expected for $H^+ + H_2$, conclusive evidence has not been reported [203, 204].

An estimation of the induction time or required delay after the bimolecular encounter to establish the statistical behaviour of the collision complex after having eliminated any possible correlation between the non-statistical approaching motion of the corresponding colliding reactants yielded a rough value of 35 fs [205]. This value, which relates to the time scale of the relaxation of the internal vibrational motions, turns out to be comparable to the average rotational period and lifetime of the intermediate complex. It is then not surprising to find that statistical approaches had already been

tested in this ion–diatom reactive collision on previous occasions. Takayanagi *et al.* [206] found that cumulative reaction probabilities for the reactive non-charge transfer $D^+ + H_2 \rightarrow DH + H^+$ process can be reproduced by a statistical prediction below the above mentioned energy of which charge-transfer mechanisms become energetically open. Analogously, a similar statistical analysis of DH_2^+ for $J=0$ concluded that the electronically adiabatic reactions for that system are mostly statistical [207]. Nevertheless a PST calculation tried in [199] was found to provide cross-sections far to agree with previous experimental measurements [202] and trajectory surface hopping calculations on the $H^+ + D_2$ reaction.

Renewed interest in these reactions has been manifested by the recent experimental investigations on the $H^+ + D_2$ reaction by means of the Rydberg H-atom TOF spectroscopy [208–210]. A comparison between the measured rotational populations of HD at 530 meV collision energy and those predicted by prior distribution theory indicates that the HD product states are, with some deviations, mainly statistically populated [208]. The preference found for the backward scattering direction on the measured angular distributions, however, was interpreted as a result of the short lifetime for the collision complex formed during the reaction. Moreover, despite the limited angular resolution of the experiments of [210] (which precluded the recording of the cross-sections in either the forward or backward scattering region), both measured and theoretical DCSs obtained by means of QCT calculations for the same reaction and the same collision energy displayed a characteristic symmetry around the sideways direction [210].

The present statistical calculations were carried out on the Aguado *et al.* PES [211].

Figures 29–31 show the reaction probabilities at $J=0$ in terms of the collision energy of the $H^+ + D_2(v=0, j=0) \rightarrow HD + D^+$, $D^+ + H_2(v=0, j=0) \rightarrow DH + H^+$, and

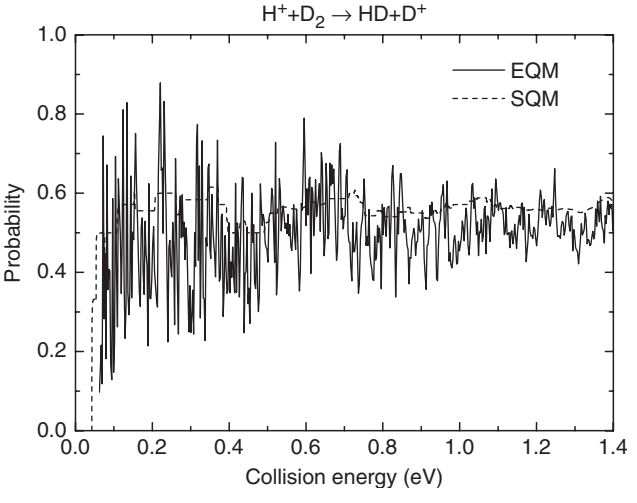

Figure 29. Total reaction probabilities at zero total angular momentum in terms of the collision energy for the $H^+ + D_2(v=0, j=0) \rightarrow HD + D^+$ reaction. The SQM result (dashed line) is compared with the WP EQM calculation (solid line) of [95].

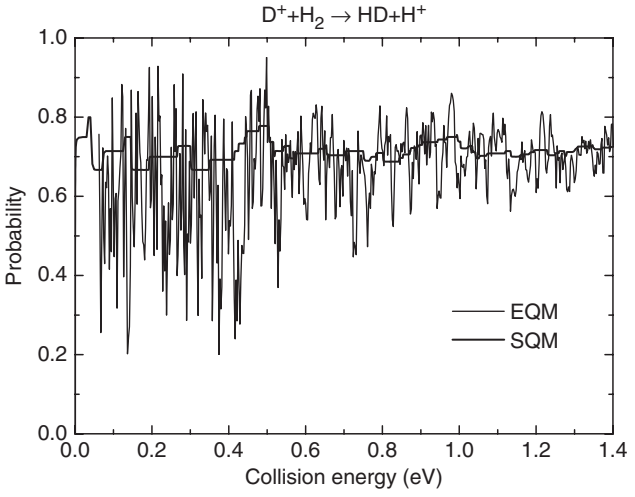

Figure 30. Same as figure 29 for the $D^+ + H_2(v = 0, j = 0) \rightarrow HD + H^+$ reaction.

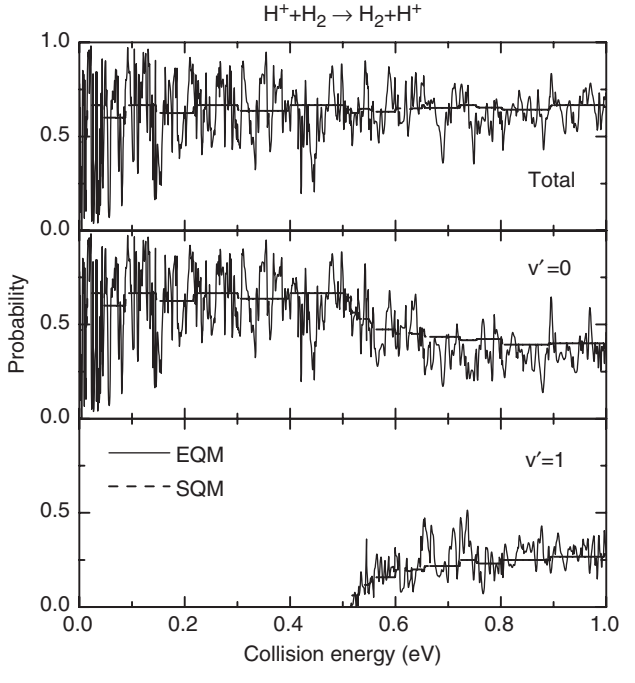

Figure 31. Reaction probabilities for the total (top panel) and final vibrational state selected $H^+ + H_2(v = 0, j = 0)$ reactions. Probabilities of forming $H_2(v' = 0)$ and $H_2(v' = 1)$ are shown in middle and bottom panels, respectively. SQM results (dashed line) are compared with TI EQM probabilities (solid line) from reference [212].

$H^+ + H_2(v = 0, j = 0) \rightarrow H_2 + H^+$ reactions, respectively. In the three cases, the SQM result is presented in comparison with probabilities from EQM calculations. In figures 29 and 30 this EQM calculation corresponds to a quantum WP approach [95] whereas for the $H^+ + H_2$ reaction in figure 31, the EQM approach is the TI method of Honvault and Launay [212]. The extremely structured probability profile obtained by means of the exact methods contrasts with the flat SQM result. The statistical prediction represents, however, a precise average description of the EQM total reaction probability, being the stepped structure result of the onset of reactant and product diatomic rovibrational states contributing to the reaction. In particular, the statistical probability experiments a decrease when a reactant channel v, j, Ω becomes energetically open, whereas a sudden increase is noticed every time a product channel v', j', Ω' becomes energetically accessible. The reason for such behaviour is the expression itself for the statistical approximation for the state-to-state probability of equation (4). In any case, the previously mentioned good average description provided by the SQM and the existence of those many narrow resonances in the probabilities obtained by the exact calculation may be perfectly understood as manifestations of an insertion-like reaction mechanism for these reactions.

As shown in the middle and bottom panels of figure 31, the good average accord between SQM and EQM reaction probabilities is extended to the case of the $H^+ + H_2(v = 0, j = 0) \rightarrow H_2(v') + H^+$ state-to-state processes with $v' = 0$ and 1, respectively. In addition, the comparison between the exact opacity function and that obtained by means of the statistical approach for this reaction at $E_c = 440$ meV collision energy, shown in figure 32, reveals once more that the SQM probabilities follow the average trend of the EQM result.

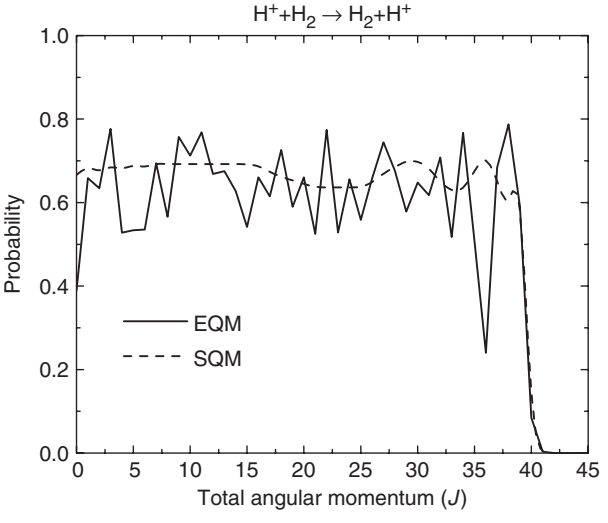

Figure 32. Opacity functions for the $H^+ + H_2(v = 0, j = 0) \rightarrow H_2 + H^+$ exchange reaction at the collision energy of 440 meV. Probabilities from the TI EQM method by Honvault and Launay [212] (solid line) and from the SQM (dashed line) are compared.

The product rotational distributions at that collision energy exhibit a statistical behaviour. The SQM yield rotationally resolved ICSs in good accord with the EQM distributions as shown in figure 33. Despite the oscillatory population found for the lower final rotational states $j' < 4$, the exact cross-section seems to be well described by the SQM prediction. Interestingly, the ICSs of figure 33 do not have the same structure as the corresponding product rotational distributions obtained for the reactions of C(^1D), N(^2D), O(^1D), and S(^1D) atoms with H_2 (see figures 4, 11, 19 and 25, respectively). For the previously analysed $X + H_2$ reactions, the rotational ICSs were found to extend to all final j' states presenting a maximum at the larger rotational states energetically accessible. For the $H^+ + H_2$ reaction the situation seems to differ somewhat for such results. Some slight inversion which favours an intermediate final rotational excitation, $j' = 2, 3$, still far from the highest state, $j' = 8$, is found. However, as it is clearly manifested in the comparison shown in figure 33, the statistical cross-section grasps the intrinsic nature of the EQM distribution. The value of the total ICS at that specific collision energy is also well described by the SQM, since the statistical prediction (23.70 Å^2) is in extremely good agreement with the EQM value (23.13 Å^2).

Another interesting dynamical feature regarding this reaction is the structure of the DCS at this collision energy of 440 meV. As shown in figure 34, the EQM angular distribution is extremely forward and backward peaked with a polarization ratio between the backward and sideways scattering direction of almost 18. A QCT result [212] also included in figure 36 shows the extreme difficulty found for classical trajectory approaches to reproduce the QM DCS. This marked dynamical feature of the angular distribution has been previously attributed to QM tunnelling through

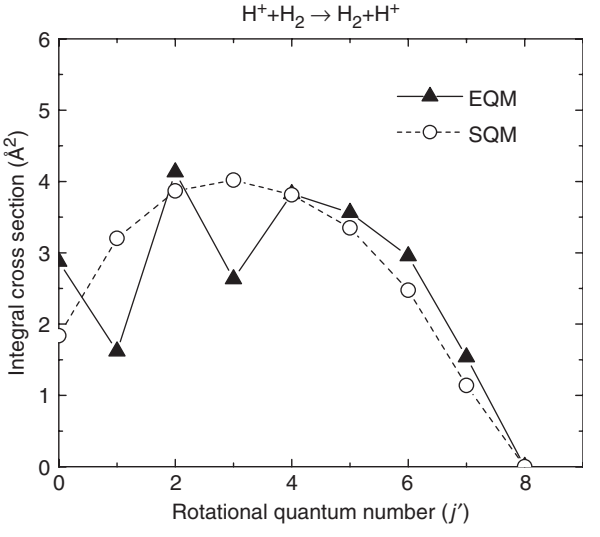

Figure 33. Rotationally resolved ICSs for the $H^+ + H_2(v = 0, j = 0) \rightarrow H_2(v' = 0, j') + H^+$ reaction at the 440 meV collision energy. The EQM results from [212] are shown as black triangles and solid line, and the SQM cross-sections are shown as black circles and dashed line.

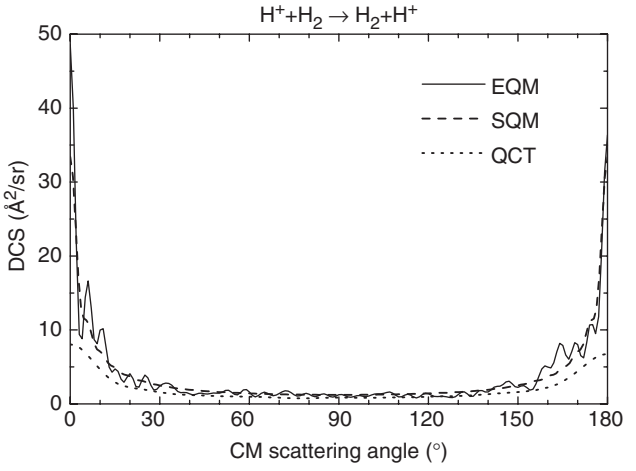

Figure 34. Total DCSs for the $H^+ + H_2(v = 0, j = 0)$ reaction at $E_c = 440$ meV collision energy obtained by means of EQM (solid line), QCT (dotted line) and SQM approaches (dashed line). Results have been taken from [212].

long-range centrifugal barriers [20] but attempts to take these contributions into account within a WKB framework in recent PST calculations could not solve the issue of the forward–backward peaks completely [75]. The SQM DCS, on the other hand, successfully reproduces the dynamics described by the exact result. With the only expected failure to describe the slight preference by the forward scattering direction existing on the EQM angular distribution (the statistical value at $\theta = 0^\circ$ results to be roughly 1.2 times lower than the EQM result) the SQM cross-section gives the right behaviour. It is worth mentioning that the preferred scattering found by the EQM calculation should be considered with caution due the extreme sensitivity of the DCSs with the collision energy and the PES employed. In this sense, it was found that EQM calculations on the PES employed in [206] at the same collision energy predict that products of the $H^+ + H_2$ reaction were mainly backscattered.

A more detailed analysis of the DCS at a state-to-state level reveals that the total angular distribution shown in figure 34 is the result of very different DCSs depending on the final rotational state of the product $H_2(v' = 0, j')$ fragment. In figure 35 EQM rotationally resolved DCSs (in solid line) are shown for $j' = 0$–7. It is found that for some final j' states ($j' = 0$, 1 and 6) DCSs present a clear preference for the forward scattering region, in some other cases, the privileged scattering direction is the opposite ($j' = 2, 5$ and 4), and finally isotropic scattering is predicted when the rotational excitation of the H_2 product fragments is $j' = 3$ and 7. The SQM approach has some difficulties in describing such a variety of different dynamical behaviours. Although the comparison with the EQM distributions improves when the final j' state increases and some specific features (such as the forward scattering maximum peak for $j' = 1$ in the top right panel of figure 35) the overall accord found is of a lower quality than that for the total reaction DCS in figure 34.

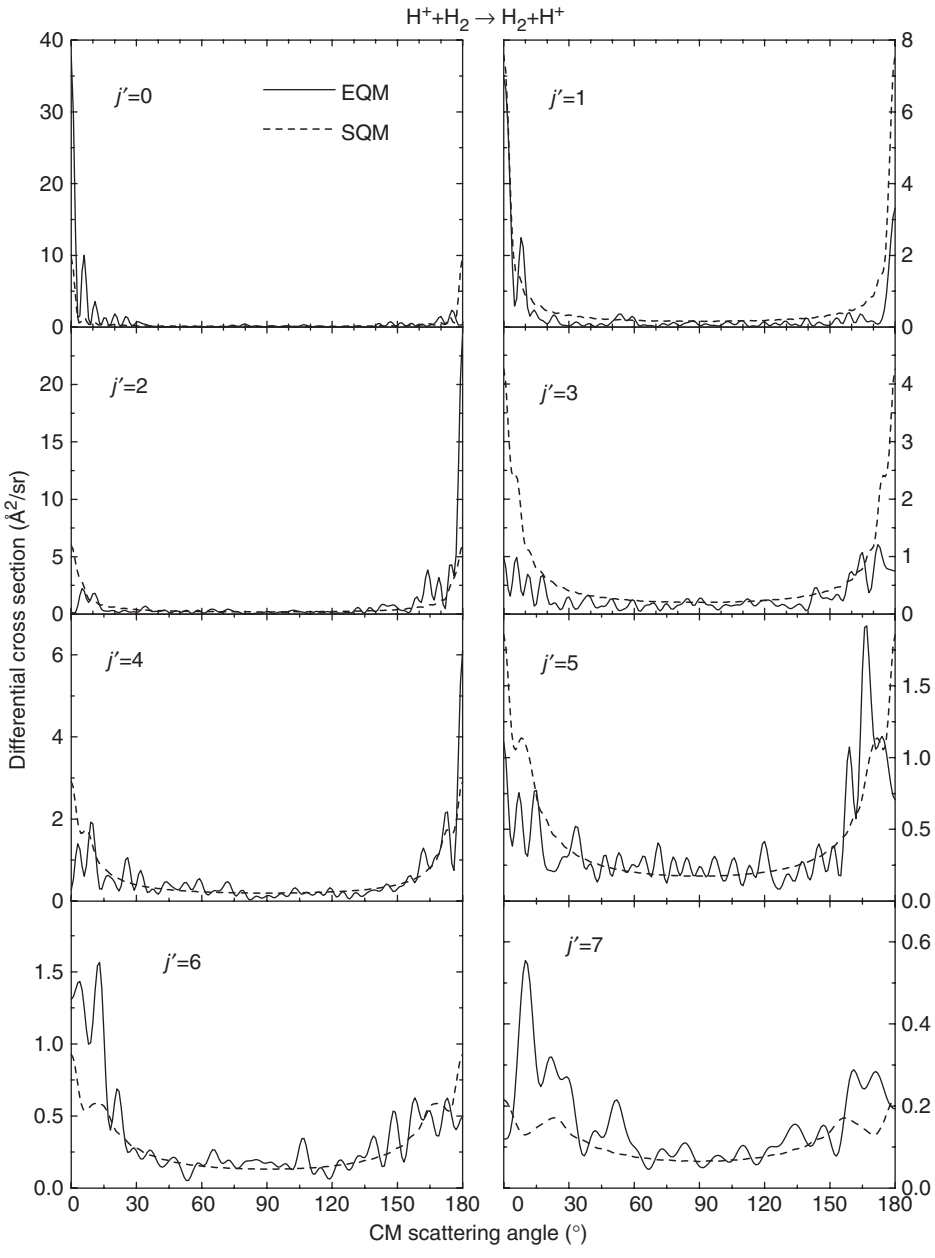

Figure 35. State-to-state DCSs for the $H^+ + H_2(v = 0, j = 0) \rightarrow H_2(v' = 0, j' = 0\text{–}7) + H^+$ exchange reaction at $E_c = 440$ meV obtained by means of EQM (solid line) and SQM (dashed line) calculations.

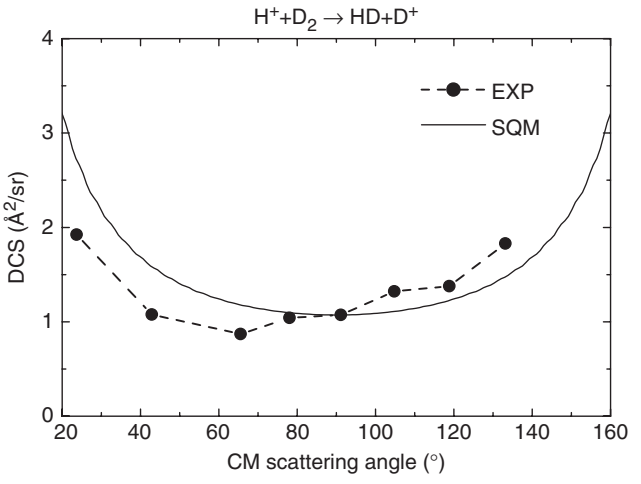

Figure 36. Total DCSs for the $H^+ + D_2(v = 0, j = 0) \rightarrow HD_2 + D^+$ reaction at $E_c = 530$ meV collision energy. The statistical cross-section (solid line) is compared with the experimental result of [210] (black circles and dashed line).

An example of the comparison with the Rydberg H-atom TOF spectroscopic measurements of the DCS at $E_c = 530$ meV on the $H^+ + D_2$ reaction [210] is presented in figure 36. The experimental distribution, which has been reported only for the limited angle range between 20° and 140°, is only partially described by the SQM result. Incidentally the statistical prediction was found to be in very good agreement with the QCT result reported in [210].

5. Competition between insertion and abstraction: H + O_2 reactions

In this final section of the results, the collisions of an H atom with O_2 are investigated by means of the SQM. The $H + O_2$ reaction is characterized by a deep potential well, with around 2.5 eV depth. As suggested in the introduction, the interest in including this process in the present review lies in the possible existence of a competition between the insertion and abstraction mechanisms during the collision. In this sense, the application of the SQM, a method which is based on the assumption of the occurrence of an insertion reaction, may be extremely helpful in distinguishing the contribution of such a reaction pathway from the overall dynamics of the process.

Indications of such a competition between two different dynamical reaction mechanisms for $H + O_2$ have been previously reported. Variations of the reaction probability in terms of the energy found in the QCT calculation by Kleinermanns and Schinke [213] were interpreted as the coexistence of a long-living complex dynamics at low energy and a direct reaction mechanism at high energy. The symmetrical scattering angle distribution around 90° at $E_c = 1.2$ eV would support the idea of an intermediate complex at a low-energy regime. In another QCT calculation [214] it was also concluded that

the reaction becomes more direct with increasing energy from the shape of final rotational distributions and the rise of backward scattering peaking, in comparison with more symmetrical distributions found at lower energies. The $J=0$ reaction probability obtained in a recent TD WP calculation [215] consisted in many sharp resonances up to $E_c \sim 1.15\,\text{eV}$. Beyond that energy, the enhancement of the reaction probability was attributed to the onset of a direct non-complex-forming reaction path. This new mechanism would thus compete in that high-energy regime with the insertion process, responsible for the much broader resonances peaks.

Experimental evidence of such a competition between insertion and abstraction for the $H + O_2$ reaction has also been reported. Thus, in a LIF spectroscopic study of the process at 1.6 eV collisional energy [216], rotational distributions for the $OH(v' = 1)$ channel and the vibrational branching ratio were found to behave statistically. On the other hand, a direct reaction pathway favours the excitation of the high rotational product states of the $OH(v' = 0)$ channel. A direct reaction pathway, on the contrary, would be responsible of the excitation of the high rotational product states of the $OH(v' = 0)$ channel. Analogously, using Doppler LIF spectroscopy, angular distributions at 1 eV collisional energy were found to be forward–backward symmetric [217], whereas the dynamical indication of a long-lived complex seemed to disappear at higher energies.

The issue of the possible statistical nature of the $H + O_2$ reaction has been extensively analysed. Although statistical approaches have failed to reproduce the energy dependence of classical trajectory ICS [218], rotational and vibrational distributions for low energies were satisfactorily described [213]. Interestingly, the calculation of the thermal rate coefficients for both the $H + O_2 \rightarrow OH + O$ reaction and its reverse were found to be affected by important non-statistical effects [66, 219]. These effects were caused by trajectories that, starting from either the $H + O_2$ or $O + OH$ valley, after forming the complex, return to the configuration space from which they came. Similar studies on the possible competition between statistical and non-statistical features were carried out using the SACM [220, 221]. Despite all these efforts to quantify the possible importance of non-statistical effects, a precise determination by means of classical trajectory methods is subject to the uncertainties introduced by the zero point energy problem [94, 219, 221, 222].

No conclusive answers about the possible statistical behaviour of the reaction were extracted from the accurate TI QM study for total angular momentum $J=0$ performed by Pack *et al*. [223]. On one hand, reaction probabilities, with many resonances, were found to spread out into many final vibrational and rotational channels in both reactant and product arrangements. But, on the other hand, non-statistical behaviour signatures were found for both resonance decays and cumulative reaction probabilities. The recent calculation [107] of the rate constant of the $H + O_2$ and $O + OH$ collisions by means of a WP version of the SQM review here may constitute nevertheless a positive test to certify the statistical nature of the processes.

A statistical calculation has been carried out on the DMBE IV PES of Varandas and coworkers [224].

The study included in this paper on the $H + O_2$ reaction also starts with the comparison of the SQM results for the reaction probability at $J=0$ with previous EQM results. In this case, in figure 37, the statistical reaction probabilities in terms of the collision

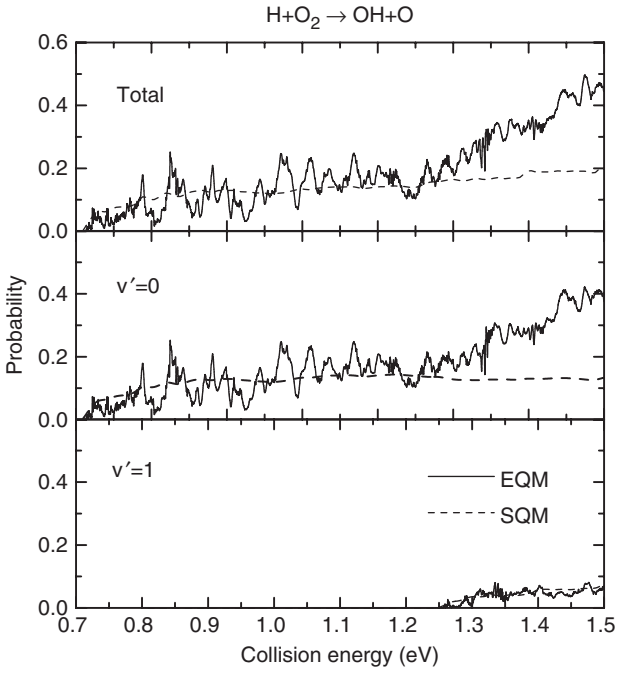

Figure 37. Reaction probabilities for the $H + O_2(v = 0, j = 1)$ reaction in terms of the collision energy at a zero total angular momentum. Total reaction probabilities are in the top panel and the vibrationally resolved reactions for production of the product OH fragment in its ground state $v' = 0$ and first excited $v' = 1$ state are in middle and bottom panels, respectively. EQM results (solid line) for the total reaction process are from the TD WP calculation by Zhang and Zhang [225] and for the vibrationally resolved reactions, TD WP calculation by Dai and Zhang [226]. SQM probabilities are shown as the dashed line.

energy are shown together with TD WP probabilities by Zhang and Zhang [225] and by Dai and Zhang [226]. The EQM total reaction probabilities [225] in the top panel of figure 37 experiment a sudden increase around 1.3 eV collision energy. The SQM result seems to reproduce the exact reaction probability at zero total angular momentum up to that particular energy, providing an average description of the TD WP result, but fails to give the correct reaction probability beyond that energy. A similar comparison between the corresponding final vibrational state-selected probabilities (in the middle and bottom panels) reveals that the origin of the discrepancies between the SQM results and the TD WP probabilities [226] lies in the process of formation of the OH fragments in their ground vibrational state. Whereas the same kind of disagreement is found for $v' = 0$, the statistical prediction reproduces both the reaction threshold for the $H + O_2(v = 0, j = 1) \rightarrow OH(v' = 1) + O$ collision at $E_c = 1.25$ eV and the average trend of the exact probability up to the highest collision energy (1.5 eV) considered in the present comparison.

In figure 38 the discrepancies between the statistical results and those from the EQM are further investigated by analysis of the state-to-state reaction probabilities for the $H + O_2(v = 0, j = 1) \rightarrow OH(v' = 0, j') + O$ processes at $J = 0$. In this case, the SQM results are compared with TD WP calculations from [226] for the final rotational

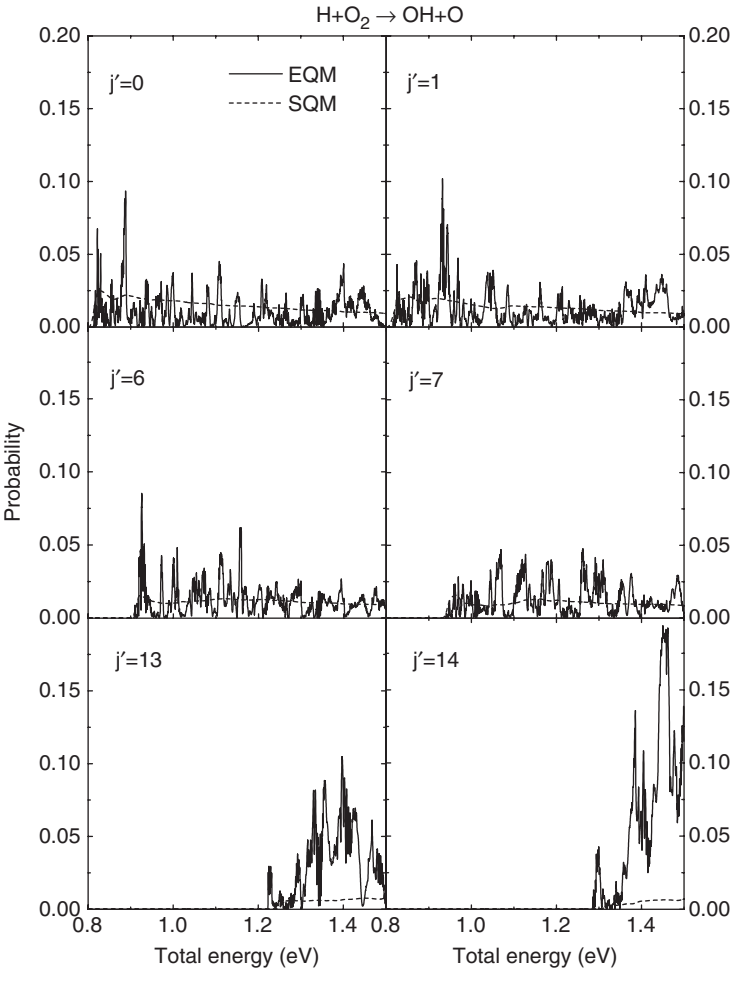

Figure 38. State-to-state reaction probabilities for the $H + O_2(v = 0, j = 1) \rightarrow OH(v' = 0, j') + O$ processes at $J = 0$. Results for the $j' = 0$ and 1 final rotational states are in the two top panels, $j' = 6$ and 7 in the middle panels and $j' = 13$ and 14 are shown in the bottom panels. Solid lines: TD WP results from [226]; dashed line: SQM reaction probabilities.

$j' = 0, 1, 6, 7, 12$ and 13 excitations of the OH fragment. It is clear from the figure that the average description provided by the SQM reaction probabilities of the TD WP results, fairly good for the lower and intermediate final rotational excitations (in the top and middle panels), is completely insufficient for the higher values of j' (13 and 14). In fact, the EQM result indicates that there is an important specificity of the process to produce large rotational excitations on the product OH fragments, which will not be possible to reproduce on statistical grounds. Moreover, the energy range for which the probability to form products with those particular final rotational excitations results extremely large is the region in which the sudden increase

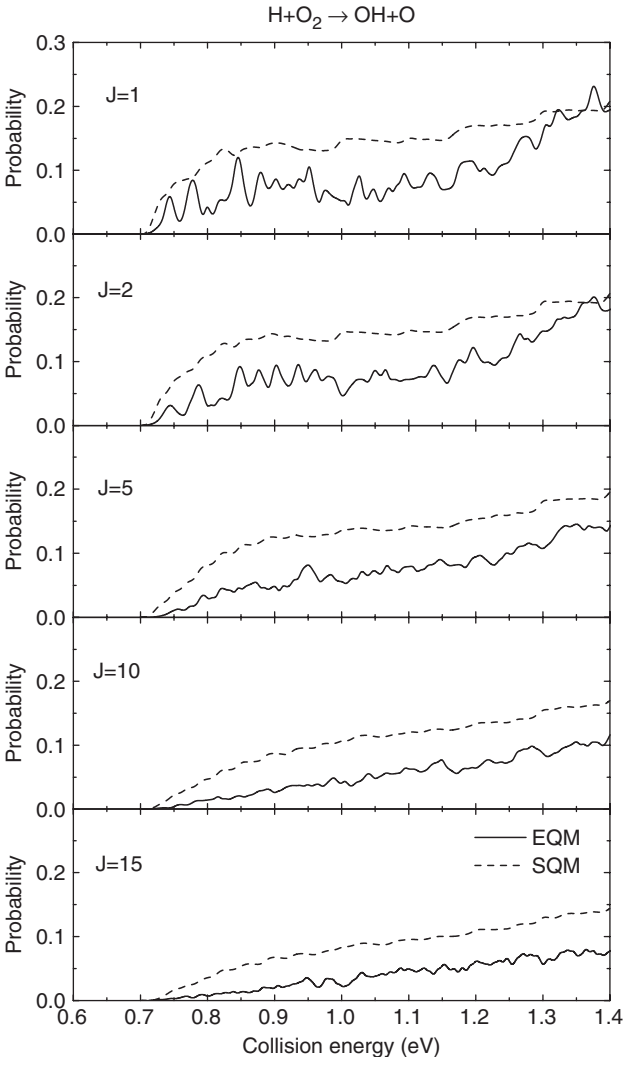

Figure 39. Total reaction probabilities for the $H + O_2(v = 0, j = 1)$ collision at total angular momentum $J = 1$, 2, 5 and 10 (from top to bottom) in terms of the collision energy. SQM probabilities (dashed line) are compared with TD WP results from Meijer and Goldfield [215, 227, 228] (solid line).

of the $J = 0$ reaction probabilities is observed (see figure 37). This would also explain the reason for the failure of the statistical approach in that energy region.

The profiles of the total reaction probabilities for $J > 0$ total angular momenta differ somewhat from the situation for $J = 0$. As shown in figure 39, where probabilities obtained by a TD WP calculation [215, 227, 228] (from top to bottom) for $J = 1, 2, 5, 10$ and 15 are presented, the narrow resonances found at low collision energies for the zero angular momentum case is replaced by less structured probability profiles. Moreover, the increase in the reactivity experimented at $J = 0$ (see figure 37) seems to

disappear and beyond $J = 5$, an almost linear dependence with the collision energy is found. The SQM predictions for the reaction probabilities at these values of the total angular momentum are included in figure 39 with a dashed line. The most characteristic aspect in their comparison with the EQM results of [215, 227, 228] is the progressive deviation from the exact result when J increases. The statistical probabilities are therefore far from representing the average value of the correct results and clearly overestimate the TD WP findings. Moreover, comparison with results for higher total angular momenta, not presented here, indicate that the situation does not improve too much. This feature might be due to deficiencies on the CS approximation assumed by the SQM, since warnings about the use of helicity decoupling methods have been previously reported [107, 227, 229]. In particular, recent applications of the WP version of the present SQM considered the reverse reaction, $OH + O \rightarrow H + O_2$, to obtain ICSs and rate constants for the $H + O_2$ process [107, 230]. Therefore, predictions obtained by means of the SQM used as in the present review should be accepted with some caution.

As a result, SQM ICSs [231] are too large in comparison with both TD WP [232] and experimental results [232–235]. It is nevertheless interesting to analyse the comparison

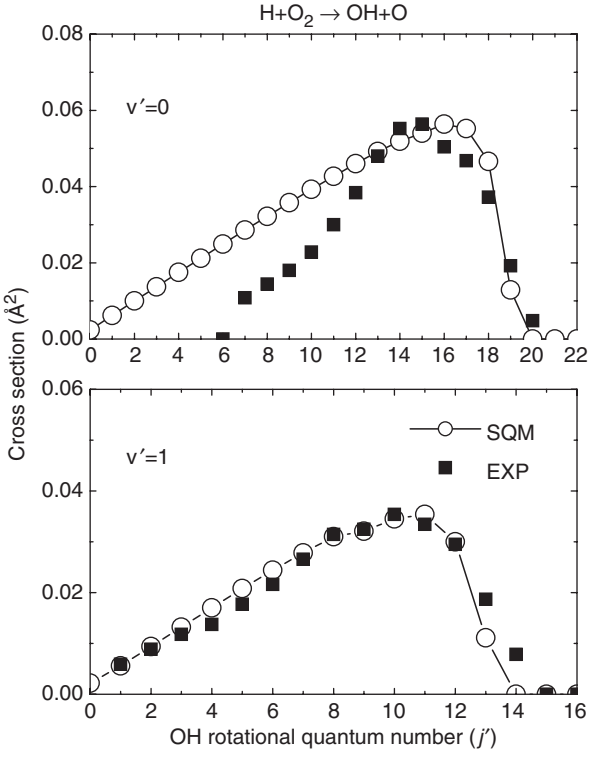

Figure 40. Product OH rotational state resolved ICSs at $E_c = 1.6$ eV for the ground OH($v' = 0$) (top panel) and first excited (bottom panel) OH($v' = 1$) vibrational states. The SQM cross-sections (empty circles and solid lines) are compared with experimental results from [216] (black squares) which were scaled with the same factor for both OH vibrational excitations.

found between the SQM rotationally resolved cross-sections and those experimentally measured by Bronikowski *et al*. [216]. The actual comparison for the $H + O_2(v = 0, j = 1) \rightarrow OH(v', j') + O$ collisions with $v' = 0$ and $v' = 1$ at a 1.6 eV collision energy are shown in figure 40. The experimental results, originally reported as relative cross-sections, were scaled to match the theoretical results with the same factor for both product vibrational excitations. From the figure the statistical character of the experimentally measured $v' = 1$ rotational distributions becomes evident. Despite the need for the actual values of the ICS given in the ordinate axis to be corroborated by an exact calculation due the problems found for the statistical predictions for high angular momenta, the SQM approach reproduces fairly well the hot rotational ICS which extends up to $j' = 14$ with a maximum around $j' = 10$. The ICSs corresponding to the formation of OH product fragments in their ground vibrational state (in the top panel), on the contrary, exhibit a slightly different behaviour. Despite the maximum also being found around the higher j' rotational states, no population is found at all up to $j' = 6$. This feature is obviously not reproduced by the monotonic increase of the final rotational states predicted by the SQM. Interestingly, signs of the non-statistical behaviour are found for the $v' = 0$ case and not for $v' = 1$, consistent with the result discussed above regarding the reaction probabilities for a zero angular momentum $J = 0$. Moreover it is worth mentioning that the present SQM results improve considerably the previous comparison of the experimental measurements with results from the PST calculation reported in [216].

6. Summary

In this work results of different studies on a variety of atom–diatom reactions by means of a recently developed statistical quantum method have been shown and discussed. First, reactive collisions of a H_2 fragment with a $C(^1D)$, $N(^2D)$, $O(^1D)$, or $S(^1D)$ atom have been considered. Then, as an example of an ion–diatom reaction, the $H^+ + H_2$ and isotope variants has been treated. Finally, a summary of preliminary results on the reaction between O_2 and a H atom has been presented.

The reliability of the statistical method to treat insertion-like reactions has been extensively discussed. Comparison with both exact quantum calculations and experiment has shown that the information provided by this theoretical approach is of great usefulness in understanding the precise nature of the dynamics of these processes. It has also been shown that the application of the method may also inform about possible deviations from collision forming mechanisms. Thus an indirect confirmation of the onset of a direct abstraction reaction pathway due to the contribution from excited potential energy surfaces can be gained, as exemplified in the $X + H_2$ processes discussed here. Moreover, for those cases for which competition between different dynamical mechanisms is expected, the statistical quantum method becomes extremely useful in establishing the limits of insertion dynamics.

The capabilities of the method have been tested by obtaining a wide list of observables and quantities such as reaction probabilities, product distributions, cross-sections, and thermal rate constants at both the total and state-to-state reaction levels.

Acknowledgment

This work has been funded by the MEC (Spain) under Grant FIS2004-02461 and the Ramón y Cajal programme. The author is sincerely grateful to D. E. Manolopoulos and E. J. Rackham for their collaboration and friendship during his stay at Oxford University. It is also a pleasure and a privilege to thank the long list of collaborators over the years devoted to the study of atom–diatom reactions: A. Aguado, F. J. Aoiz, P. N. Arenas, N. Balucani, L. Bañares, P. Bargueño, L. Bonnet, P. Casavecchia, F. Dayou, V. J. Herrero, P. Honvault, J.-M. Launay, P. Larrégaray, M. Paniagua, J. C. Rayez, O. Roncero and I. Tanarro.

References

[1] M. Gruebele, I. R. Sims, E. D. Potter, and A. H. Zewail, J. Chem. Phys. **95,** 7763 (1991).
[2] I. R. Sims, M. Gruebele, E. D. Potter, and A. H. Zewail, J. Chem. Phys. **97,** 4127 (1992).
[3] D. Zhong, P. Y. Cheng, and A. H. Zewail, J. Chem. Phys. **105,** 7864 (1996).
[4] J. C. Williamson, J. Cao, H. Ihee, H. Frey, and A. H. Zewail, Nature **386,** 159 (1997).
[5] P. Casavecchia, N. Balucani, and G. G. Volpi, Annu. Rev. Phys. Chem. **50,** 347 (1999).
[6] K. Liu, Annu. Rev. Phys. Chem. **52,** 139 (2001).
[7] X. Liu, J. J. Harich, G. C. Schatz, and X. Yang, Science **289,** 1536 (2000).
[8] S. C. Althorpe, Int. Rev. Phys. Chem. **23,** 219 (2004).
[9] S. C. Althorpe, Chem. Phys. Lett. **370,** 443 (2003).
[10] S. C. Althorpe, J. Phys. Chem. A **107,** 7152 (2003).
[11] S. C. Althorpe, F. Fernández-Alonso, B. D. Bean, J. D. Ayers, A. E. Pomerantz, R. N. Zare, and E. Wrede, Nature **416,** 67 (2002).
[12] S. C. Althorpe, J. Chem. Phys. **117,** 4623 (2002).
[13] R. T. Skodje, D. Skouteris, D. E. Manolopoulos, S.-H. Lee, F. Dong, and K. Liu, Phys. Rev. Lett. **85,** 1206 (2000).
[14] R. T. Skodje, D. Skouteris, D. E. Manolopoulos, S.-H. Lee, F. Dong, and K. Liu, J. Chem. Phys. **112,** 4536 (2000).
[15] K. Liu, R. T. Skodje, and D. E. Manolopoulos, Phys. Chem. Chem. Phys. **5,** 27 (2002).
[16] F. Fernández-Alonso, B. D. Bean, J. D. Ayers, A. E. Pomerantz, R. N. Zare, F. J. Aoiz, and L. Bañares, Ang. Chem. Int. Ed. **39,** 2748 (2000).
[17] D. E. Manolopoulos, Nature **419,** 266 (2002).
[18] S. A. Harich, D. Dai, C. C. Wang, S. D. Chao, and R. Skodje, Nature **419,** 281 (2002).
[19] E. J. Rackham, F. Huarte-Larrañaga, and D. E. Manolopoulos, Chem. Phys. Lett. **343,** 356 (2001).
[20] E. J. Rackham, T. González-Lezana, and D. E. Manolopoulos, J. Chem. Phys. **119,** 12895 (2003).
[21] L. Wolfenstein, Phys. Rev. **82,** 690 (1951).
[22] W. Hauser and H. Feshbach, Phys. Rev. **87,** 366 (1952).
[23] R. M. Eisberg and N. M. Hintz, Phys. Rev. **103,** 645 (1956).
[24] B. L. Cohen, Phys. Rev. **92,** 1245 (1953).
[25] L. Rosen and L. Stewart, Phys. Rev. **99,** 1052 (1955).
[26] W. W. Pratt, Phys. Rev. **94,** 1086 (1954).
[27] J. C. Keck, J. Chem. Phys. **29,** 410 (1958).
[28] J. Keck and A. Kalelkar, J. Chem. Phys. **49,** 3211 (1968).
[29] R. B. Bernstein, A. Dalgarno, H. Massey, and I. C. Percival, Proc. Roy. Soc. London, Ser. A **274,** 427 (1963).
[30] D. R. Herschbach, Disc. Faraday Soc. **33,** 149 (1962).
[31] W. B. Miller, S. A. Safron, and D. R. Herschbach, Disc. Faraday Soc. **44,** 108 (1967).
[32] S. K. Kim and D. R. Herschbach, Faraday Disc. Chem. Soc. **84,** 159 (1987).
[33] D. O. Ham and J. L. Kinsey, J. Chem. Phys. **48,** 939 (1967).
[34] D. O. Ham and J. L. Kinsey, J. Chem. Phys. **53,** 285 (1970).
[35] S. J. Riley and D. R. Herschbach, J. Chem. Phys. **58,** 27 (1973).
[36] T. Horie and T. Kasuga, J. Chem. Phys. **40,** 1683 (1964).

[37] W. B. Miller, S. A. Safron, and D. R. Herschbach, J. Chem. Phys. **56,** 3581 (1972).
[38] S. A. Safron, N. D. Weinstein, D. R. Herschbach, and J. C. Tully, Chem. Phys. Lett. **12,** 564 (1972).
[39] J. C. Light, J. Chem. Phys. **40,** 3221 (1964).
[40] P. Pechukas and J. C. Light, J. Chem. Phys. **42,** 3281 (1964).
[41] J. C. Light and J. Lin, J. Chem. Phys. **43,** 3209 (1965).
[42] J. Lin and J. C. Light, J. Chem. Phys. **45,** 2545 (1966).
[43] P. Pechukas, J. C. Light, and C. Rankin, J. Chem. Phys. **44,** 794 (1966).
[44] J. C. Light, Discuss. Faraday Soc. **44,** 14 (1967).
[45] R. A. White and J. C. Light, J. Chem. Phys. **53,** 379 (1971).
[46] W. H. Miller, J. Chem. Phys. **52,** 543 (1970).
[47] H. Eyring, J. Chem. Phys. **3,** 107 (1935).
[48] K. Yang and T. Ree, J. Chem. Phys. **35,** 588 (1961).
[49] R. A. Marcus, J. Chem. Phys. **20,** 359 (1952).
[50] R. A. Marcus, J. Chem. Phys. **20,** 364 (1952).
[51] R. A. Marcus, J. Chem. Phys. **45,** 2630 (1966).
[52] R. A. Marcus, J. Chem. Phys. **53,** 604 (1970).
[53] W. H. Wong and R. A. Marcus, J. Chem. Phys. **55,** 5625 (1971).
[54] G. Worry and R. A. Marcus, J. Chem. Phys. **67,** 1636 (1977).
[55] R. D. Levine, *Molecular Reaction Dynamics* (Cambridge University Press, Cambridge, 2005).
[56] P. Pechukas and F. J. McLafferty, J. Chem. Phys. **58,** 1622 (1973).
[57] E. Pollak and P. Pechukas, J. Chem. Phys. **69,** 1218 (1978).
[58] W. H. Miller, J. Chem. Phys. **65,** 2216 (1976).
[59] E. Pollak and P. Pechukas, J. Chem. Phys. **70,** 325 (1979).
[60] E. Pollak and R. D. Levine, J. Chem. Phys. **72,** 2990 (1980).
[61] A. F. Wagner and E. K. Parks, J. Chem. Phys. **65,** 4343 (1976).
[62] D. L. Bunker and T.-S. Chang, J. Phys. Chem. **73,** 943 (1969).
[63] D. M. Wardlaw and R. A. Marcus, Adv. Chem. Phys. **70,** 231 (1988).
[64] J. B. Anderson, J. Chem. Phys. **58,** 4684 (1973).
[65] G. M. Wieder and R. A. Marcus, J. Chem. Phys. **37,** 1835 (1962).
[66] R. A. Marcus, J. Chem. Phys. **85,** 5035 (1986).
[67] J. J. Sloan, J. Phys. Chem. **92,** 18 (1988).
[68] P. Larrégaray, L. Bonnet, and J. C. Rayez, J. Chem. Phys. **114,** 3349 (2001).
[69] P. Larrégaray, L. Bonnet, and J. C. Rayez, Phys. Chem. Chem. Phys. **4,** 1577 (2002).
[70] P. Larrégaray, L. Bonnet, and J. C. Rayez, Phys. Chem. Chem. Phys. **4,** 1781 (2002).
[71] L. Bonnet, P. Larrégaray, and J. C. Rayez, Phys. Chem. Chem. Phys. **7,** 3540 (2005).
[72] L. Bonnet, P. Larrégaray, and J. C. Rayez, Chem. Phys. Lett. **383,** 288 (2004).
[73] L. Bonnet, J. C. Rayez, and Ph. Halvick, J. Chem. Phys. **99,** 1771 (1993).
[74] L. Bonnet and J. C. Rayez, Phys. Chem. Chem. Phys. **1,** 2383 (1999).
[75] P. Larrégaray, L. Bonnet and J. C. Rayez, J. Phys. Chem. A **110,** 1552 (2006).
[76] M. Quack and J. Troe, Ber. Bunsenges. Phys. Chem. **78,** 240 (1970).
[77] M. Quack and J. Troe, Ber. Bunsenges. Phys. Chem. **79,** 171 (1975).
[78] M. Quack and J. Troe, Ber. Bunsenges. Phys. Chem. **79,** 469 (1975).
[79] R. D. Levine and B. R. Johnson, Chem. Phys. Lett. **4,** 365 (1969).
[80] W. H. Miller, J. Chem. Phys. **50,** 931 (1969).
[81] R. D. Levine, Disc. Faraday Soc. **44,** 82 (1967).
[82] L. Holmlid and K. Rynefors, Chem. Phys. **77,** 6346 (1982).
[83] K. Rynefors, Computer Phys. Commun. **27,** 201 (1982).
[84] K. Rynefors and L. Holmlid, Chem. Phys. **60,** 405 (1981); Erratum: Chem. Phys. **74,** 446 (1983).
[85] K. Rynefors, P. A. Elofson, and L. Holmild, Chem. Phys. **90,** 347 (1984).
[86] P. A. Elofson, K. Rynefors, and L. Holmlid, Chem. Phys. **118,** 1 (1987).
[87] L. Holmlid and P. A. Elofson, Faraday Discuss. Chem. Soc. **84,** 95 (1987).
[88] P. A. Elofson and L. Holmlid, Chem. Phys. Lett. **166,** 112 (1990).
[89] See discussion in Faraday Discuss. Chem. Soc. **84,** 87 (1987).
[90] A. Lee, R. L. LeRoy, Z. Herman, R. Wolfgang, and J. C. Tully, Chem. Phys. Lett. **12,** 569 (1972).
[91] See discussion on Disc. Faraday Soc. **44,** 80 (1967).
[92] R. D. Levine, B. R. Johnson, and R. B. Bernstein, Chem. Phys. Lett. **19,** 1 (1973).
[93] J. A. Miller, J. Phys. Chem. **84,** 6170 (1986).
[94] L. A. M. Quintales, A. J. C. Varandas, and J. M. Alvariño, J. Phys. Chem. **92,** 4552 (1988).
[95] T. González-Lezana, A. Aguado, M. Paniagua, and O. Roncero, J. Chem. Phys. **123,** 194309 (2005).

[96] N. Balucani, G. Capozza, E. Segoloni, A. Russo, R. Bobbenkamp, P. Casavecchia, T. González-Lezana, E. J. Rackham, L. Bañares, and F. J. Aoiz, J. Chem. Phys. **122,** 234309 (2005).
[97] L. Bañares, F. J. Aoiz, T. González-Lezana, V. J. Herrero, and I. Tanarro, J. Chem. Phys. **123,** 224301 (2005).
[98] N. Balucani, P. Casavecchia, L. Bañares, F. J. Aoiz, T. González-Lezana, P. Honvault, and J.-M. Launay, J. Phys. Chem. A **110,** 817 (2006).
[99] R. T. Pack, J. Chem. Phys. **60,** 633 (1974).
[100] P. McGuire and D. J. Kouri, J. Chem. Phys. **60,** 2488 (1974).
[101] K. McLenithan and D. Secrest, J. Chem. Phys. **80,** 2480 (1984).
[102] B. R. Johnson, J. Comput. Phys. **13,** 445 (1973).
[103] D. C. Clary and J. P. Henshaw, Faraday Discuss. Chem. Soc. **84,** 333 (1987).
[104] S. Y. Lin and H. Guo, J. Chem. Phys. **120,** 9907 (2004).
[105] S. Y. Lin and H. Guo, J. Phys. Chem. A **108,** 10066 (2004).
[106] S. Y. Lin and H. Guo, J. Chem. Phys. **122,** 074304 (2005).
[107] S. Y. Lin, E. J. Rackham, and H. Guo, J. Phys. Chem. A **110,** 1534 (2006).
[108] M. H. Alexander, E. J. Rackham, and D. E. Manolopoulos, J. Chem. Phys. **121,** 5221 (2004).
[109] S. Atahan, M. H. Alexander, and E. J. Rackham, J. Chem. Phys. **123,** 204306 (2005).
[110] F. J. Aoiz, L. Bañares, and V. J. Herrero, J. Phys. Chem. A (in press).
[111] N. Balucani, G. Capozza, F. Leonori, E. Segoloni, and P. Casavecchia, Int. Rev. Phys. Chem. **25,** 109 (2006).
[112] R. J. Blint and M. D. Newton, Chem. Phys. Lett. **32,** 178 (1975).
[113] G. A. Jursich and J. R. Wiesenfeld, Chem. Phys. Lett. **110,** 14 (1984).
[114] W. H. Fisher, T. Carrington, C. M. Sadowski, and C. H. Dugan, Chem. Phys. **97,** 433 (1985).
[115] D. C. Scott, J. de Juan, D. C. Robie, D. Schwartz-Lavi, and H. Reisler, J. Phys. Chem. **96,** 2509 (1992).
[116] K. Sato, N. Ishida, T. Kurakata, A. Iwasaki, and S. Tsunashima, Chem. Phys. **237,** 195 (1998).
[117] L. B. Harding, R. Guadagnini, and G. C. Schatz, J. Phys. Chem. **97,** 5472 (1993).
[118] K. Mikulecky and K.-H. Gericke, J. Chem. Phys. **98,** 1244 (1993).
[119] A. Bergeat, L. Cartechini, N. Balucani, G. Capozza, L. F. Phillips, P. Casavecchia, G. G. Volpi, L. Bonnet, and J.-C. Rayez, Chem. Phys. Lett. **327,** 197 (2000).
[120] B. Bussery-Honvault, P. Honvault, and J.-M. Launay, J. Chem. Phys. **115,** 10701 (2001).
[121] S. Y. Lin and H. Guo, J. Chem. Phys. **119,** 11602 (2003).
[122] S. Y. Lin and H. Guo, J. Phys. Chem. A **108,** 2141 (2004).
[123] L. Bañares, F. J. Aoiz, B. Bussery-Honvault, P. Honvault, and J.-M. Launay, J. Chem. Phys. **118,** 565 (2003).
[124] N. Balucani, G. Capozza, L. Cartechini, A. Bergeat, R. Bobbenkamp, P. Casavecchia, F. Javier Aoiz, L. Bañares, P. Honvault, B. Bussery-Honvault, and J.-M. Launay, Phys. Chem. Chem. Phys. **6,** 4957 (2004).
[125] P. Honvault, B. Bussery-Honvault, J.-M. Launay, F. J. Aoiz, and L. Bañares, J. Chem. Phys. **124,** 154314 (2006).
[126] J. A. Dodd, S. J. Lipson, D. J. Flanagan, and W. A. M. Blumberg, J. Chem. Phys. **94,** 4301 (1991).
[127] T. Suzuki, Y. Shihira, T. Sato, H. Umemoto, and S. Tsunashima, J. Chem. Soc. Faraday Trans. **89,** 995 (1993).
[128] H. Kobayashi, T. Takayanagi, K. Yokoyama, T. Sato, and S. Tsunashima, J. Chem. Soc. Faraday Trans. **91,** 3771 (1995).
[129] T. Takayanagi, H. Kobayashi, and S. Tsunashima, J. Chem. Soc. Faraday Trans. **92,** 1311 (1996).
[130] H. Umemoto and K.-I. Matsumoto, J. Chem. Phys. **104,** 9640 (1996).
[131] H. Umemoto, T. Asai, and Y. Kimura, J. Chem. Phys. **106,** 4985 (1997).
[132] H. Umemoto, Chem. Phys. Lett. **292,** 594 (1998).
[133] H. Kobayashi, T. Takayanagi, and S. Tsunashima, Chem. Phys. Lett. **277,** 20 (1997).
[134] L. A. Pederson, G. C. Schartz, T.-S. Ho, T. Hollebeek, H. Rabitz, L. B. Harding, and G. Lendvay, J. Chem. Phys. **110,** 9091 (1999).
[135] P. Honvault and J.-M. Launay, J. Chem. Phys. **111,** 6665 (1999).
[136] H. Umemoto, N. Terada, and K. Tanaka, J. Chem. Phys. **112,** 5762 (2000).
[137] M. Alagia, N. Balucani, L. Cartechini, P. Casavecchia, G. G. Volpi, L. A. Pederson, G. C. Schatz, L. B. Harding, T. Hollebeek, T.-S. Ho, and H. Rabitz, J. Chem. Phys. **110,** 8857 (1999).
[138] N. Balucani, M. Alagia, L. Cartechini, P. Casavecchia, G. G. Volpi, L. A. Pederson, and G. C. Schatz, J. Phys. Chem. A **105,** 2414 (2001).
[139] A. Kowalski, B. Pranszke, S. Werbowy, and Ch. Ottinger, Chem. Phys. Lett. **389,** 218 (2004).
[140] N. Balucani, L. Cartechini, G. Capozza, E. Segoloni, P. Casavecchia, G. G. Volpi, F. J. Aoiz, L. Bañares, P. Honvault, and J.-M. Launay, Phys. Rev. Lett. **89,** 013201 (2002).

[141] S. Y. Lin and H. Guo, J. Chem. Phys. **124,** 031101 (2006).
[142] T.-S. Chun, K.-L. Han, and A. J. C. Varandas, J. Phys. Chem. A **110,** 1666 (2006).
[143] A. J. C. Varandas, T.-S. Chu, K.-L. Han, and P. J. S. B. Caridade, Chem. Phys. Lett. **421,** 415 (2006).
[144] A. C. Luntz, R. Schinke, W. A. Lester Jr, and Hs. H. Günthard, J. Chem. Phys. **70,** 5908 (1979).
[145] G. K. Smith and J. E. Butler, J. Chem. Phys. **73,** 2243 (1980).
[146] G. M. Jursich and J. R. Wiesenfeld, Chem. Phys. Lett. **119,** 511 (1985).
[147] J. E. Butler, G. M. Jursich, I. A. Watson, and J. R. Wiesenfeld, J. Chem. Phys. **84,** 5365 (1986).
[148] K. Rynefors, P. A. Elofson, and L. Holmlid, Chem. Phys. **100,** 53 (1985).
[149] C. B. Cleveland, G. M. Jursich, M. Troiler, and J. R. Wiesenfeld, J. Chem. Phys. **86,** 3253 (1986).
[150] Y. Huang, Y. Gu, C. Liu, X. Yang, and Y. Tao, Chem. Phys. Lett. **127,** 432 (1986).
[151] K. Mikulecky and K.-H. Gericke, J. Chem. Phys. **96,** 7490 (1992).
[152] K. Mikulecky and K.-H. Gericke, Chem. Phys. **175,** 13 (1993).
[153] J. E. Butler, R. G. MacDonald, D. J. Donaldson, and J. J. Sloan, Chem. Phys. Lett. **95,** 183 (1983).
[154] P. M. Aker and J. J. Sloan, J. Chem. Phys. **85,** 1412 (1986).
[155] R. J. Buss, P. Casavecchia, T. Hirooka, S. J. Sibener, and Y. T. Lee, Chem. Phys. Lett. **82,** 386 (1981).
[156] R. Schinke and W. A. Lester Jr, J. Chem. Phys. **72,** 3752 (1980).
[157] P. A. Whitlock, J. T. Muckerman, and E. R. Fisher, J. Chem. Phys. **76,** 4468 (1982).
[158] S. W. Ransome and J. S. Wright, J. Chem. Phys. **71,** 6346 (1982).
[159] P. A. Elofson, K. Rynefors, and L. Holmlid, Chem. Phys. **100,** 39 (1985).
[160] M. S. Fitzcharles and G. C. Schartz, J. Phys. Chem. **90,** 3634 (1986).
[161] Y. Matsumi, K. Tonokura, M. Kawasaki, and H. L. Kim, J. Chem. Phys. **96,** 10622 (1992).
[162] R. K. Talukdar and A. R. Ravishankara, Chem. Phys. Lett. **253,** 177 (1996).
[163] Y.-T. Hsu, K. Liu, L. A. Pederson, and G. C. Schatz, J. Chem. Phys. **111,** 7921 (1999).
[164] K. Tsukiyama, B. Katz, and R. Bersohn, J. Chem. Phys. **83,** 2889 (1985).
[165] L. J. Dunne, Chem. Phys. Lett. **185,** 535 (1989).
[166] P. A. Berg, J. J. Sloan, and P. J. Kuntz, J. Chem. Phys. **95,** 8036 (1991).
[167] D.-C. Che and K. Liu, J. Chem. Phys. **103,** 5164 (1995).
[168] Y.-T. Hsu, J.-H. Wang, and K. Liu, J. Chem. Phys. **107,** 2351 (1997).
[169] Y.-T. Hsu, K. Liu, L. A. Pederson, and G. C. Schatz, J. Chem. Phys. **111,** 7931 (1999).
[170] P. Hermine, Y.-T. Hsu, and K. Liu, Phys. Chem. Chem. Phys. **2,** 581 (2000).
[171] G. C. Schatz, A. Papaioannou, L. A. Pederson, L. B. Harding, T. Hollebek, T.-S. Ho, and H. Rabitz, J. Chem. Phys. Chem. **107,** 2340 (1997).
[172] T. Peng, D. H. Zhang, J. Z. H. Zhang, and R. Schinke, Chem. Phys. Lett. **248,** 37 (1996).
[173] A. J. Alexander, F. J. Aoiz, M. Brouard, and J. P. Simons, Chem. Phys. Lett. **256,** 561 (1996).
[174] M. Alagia, N. Balucani, L. Cartechini, E. H. van Kleef, G. G. Volpi, P. J. Kuntz, and J. J. Sloan, J. Chem. Phys. **108,** 6698 (1998).
[175] A. J. Alexander, D. A. Blunt, M. Brouard, J. P. Simmons, F. Javier Aoiz, L. Bañares, Y. Fujimura, and M. Tsubouchi, Faraday Discuss. **108,** 375 (1997).
[176] F. J. Aoiz, L. Bañares, and V. J. Herrero, Chem. Phys. Lett. **310,** 277 (1999).
[177] F. J. Aoiz, L. Bañares, M. Brouard, J. F. Castillo, and V. J. Herrero, J. Chem. Phys. **113,** 5339 (2000).
[178] F. J. Aoiz, L. Bañares, J. F. Castillo, V. J. Herrero, B. Martínez-Haya, P. Honvault, J.-M. Launay, X. Liu, J. J. Lin, S. A. Harich, C. C. Wang, and X. Yang, J. Chem. Phys. **116,** 10692 (2002).
[179] F. J. Aoiz, L. Bañares, J. F. Castillo, M. Brouard, W. Denzer, C. Vallance, P. Honvault, J.-M. Launay, A. J. Dobbyn, and P. J. Knowles, Phys. Rev. Lett. **86,** 1729 (2001).
[180] X. Yang, Int. Rev. Phys. Chem. **24,** 37 (2005).
[181] X. Liu, J. J. Lin, S. Harich, G. C. Schatz, and X. Yang, Science **289,** 1536 (2000).
[182] X. Liu, J. J. Lin, S. Harich, and X. Yang, Phys. Rev. Lett. **86,** 408 (2001).
[183] X. Liu, J. J. Lin, S. Harich, and X. Yang, J. Chem. Phys. **113,** 1325 (2000).
[184] K. Yuan, Y. Cheng, X. Liu, S. Harich, X. Yang, and D. H. Zhang, Phys. Rev. Lett. **96,** 103202 (2006).
[185] A. J. Dobbyn and P. J. Knowles, Mol. Phys. **91,** 1107 (1997).
[186] A. J. Dobbyn and P. J. Knowles, Faraday Discuss. **110,** 247 (1998).
[187] P. Honvault and J.-M. Launay, J. Chem. Phys. **114,** 1057 (2000).
[188] S.-H. Lee and K. Liu, Chem. Phys. Lett. **290,** 323 (1998).
[189] S.-H. Lee and K. Liu, J. Phys. Chem. A **102,** 8637 (1998).
[190] S.-H. Lee and K. Liu, Appl. Phys. B **71,** 627 (2000).
[191] A. S. Zyubin, A. M. Mebel, S. D. Chao, and R. T. Skodje, J. Chem. Phys. **114,** 320 (2001).
[192] S. D. Chao and R. T. Skodje, J. Phys. Chem. A **105,** 2474 (2001).
[193] T.-S. Ho, T. Hollebeek, H. Rabitz, S. D. Chao, R. T. Skodje, A. S. Zyubin, and A. M. Mebel, J. Chem. Phys. **116,** 4124 (2002).
[194] L. Bañares, F. J. Aoiz, P. Honvault, and J.-M. Launay, J. Phys. Chem. A **108,** 1616 (2004).

[195] A. H. H. Chang and S. H. Lin, Chem. Phys. Lett. **320,** 161 (2000).
[196] P. Honvault and J.-M. Launay, Chem. Phys. Lett. **370,** 371 (2003).
[197] L. Bañares, J. F. Castillo, P. Honvault, and J.-M. Launay, Phys. Chem. Chem. Phys. **7,** 627 (2005).
[198] I. G. Csizmadia, J. C. Polanyi, A. C. Roach, and W. H. Wong, Can. J. Chem. **47,** 4097 (1969).
[199] J. R. Krenos, R. K. Preston, R. Wolfgang, and J. C. Tully, J. Chem. Phys. **60,** 1634 (1973).
[200] D. Gerlich, U. Nowotny, Ch. Schlier, and E. Teloy, Chem. Phys. **47,** 245 (1980).
[201] A. Ichihara, T. Shirai, and K. Yokoyama, J. Chem. Phys. **105,** 1857 (1996).
[202] M. G. Holliday, J. T. Muckerman, and L. Friedman, J. Chem. Phys. **54,** 1058 (1971).
[203] J. Krenos and R. Wolfgang, J. Chem. Phys. **52,** 5961 (1970).
[204] R. K. Preston and J. C. Tully, J. Chem. Phys. **54,** 4297 (1971).
[205] O. Brass and C. Schiler, J. Chem. Soc. Faraday Trans. **89,** 1533 (1993).
[206] T. Takayanagi, Y. Kurosaki, and A. Ichihara, J. Chem. Phys. **112,** 2615 (2000).
[207] H. Kamisaka, W. Bian, K. Nobusada, and H. Nakamura, J. Chem. Phys. **116,** 654 (2002).
[208] E. Wrede, L. Schnieder, K. Seekamp-Schnieder, B. Niederjohann, and K. H. Welge, Phys. Chem. Chem. Phys. **7,** 1577 (2005).
[209] D. Dai, C. C. Wang, G. Wu, S. A. Harich, H. Song, M. Hayes, R. T. Skodje, X. Wang, D. Gerlich, and X. Yang, Phys. Rev. Lett. **95,** 013201 (2005).
[210] H. Song, D. Dai, G. Wu, C. C. Wang, S. A. Harich, M. Hayes, X. Wang, D. Gerlich, X. Yang, and R. T. Skodje, J. Chem. Phys. **123,** 074314 (2005).
[211] A. Aguado, O. Roncero, C. Tablero, C. Sanz, and M. Paniagua, J. Chem. Phys. **112,** 1240 (2000).
[212] T. González-Lezana, O. Roncero, P. Honvault, J.-M. Launay, N. Bulut, F. J. Aoiz, and L. Bañares, J. Chem. Phys. **125,** 094314 (2006).
[213] K. Kleinermanns and J. Wolfrum, J. Chem. Phys. **80,** 1446 (1983).
[214] A. J. C. Varandas, J. Chem. Phys. **99,** 1076 (1993).
[215] A. J. H. Meijer and E. M. Goldfield, J. Chem. Phys. **108,** 5404 (1998).
[216] M. J. Bronikowski, R. Zhang, D. J. Rakestraw, and R. N. Zare, Chem. Phys. Lett. **156,** 7 (1989).
[217] R. Fei, X. S. Zheng, and G. E. Hall, J. Phys. Chem. A **101,** 2541 (1997).
[218] J. A. Miller, J. Chem. Phys. **74,** 5120 (1981).
[219] J. A. Miller and B. C. Garret, Int. J. Chem. Kinet. **29,** 275 (1997).
[220] L. B. Harding, A. I. Maergoiz, J. Troe, and V. G. Ushakov, J. Chem. Phys. **113,** 11019 (2000).
[221] J. Troe and V. G. Ushakov, J. Chem. Phys. **115,** 3621 (2001).
[222] G. Nyman, Chem. Phys. **173,** 159 (1993).
[223] R. T. Pack, E. A. Butcher, and G. A. Parker, J. Chem. Phys. **102,** 5998 (1995).
[224] M. R. Pastrana, L. A. M. Quintales, J. Brandão, and A. J. Varandas, J. Phys. Chem. **94,** 8073 (1990).
[225] D. H. Zhang and J. Z. H. Zhang, J. Chem. Phys. **101,** 3671 (1994).
[226] J. Dai and J. Z. H. Zhang, J. Phys. Chem. **100,** 6898 (1996).
[227] A. J. H. M. Meijer and E. M. Goldfield, J. Chem. Phys. **110,** 870 (1999).
[228] E. M. Goldfield and A. J. H. M. Meijer, J. Chem. Phys. **113,** 11055 (2000).
[229] D. E. Skinner, T. C. Germann, and W. H. Miller, J. Phys. Chem. A **102,** 3828 (1998).
[230] C. Xu, D. Xie, D. H. Zhang, S. Y. Lin, and H. Guo, J. Chem. Phys. **122,** 244305 (2005).
[231] P. Bargueño, T. González-Lezana, P. Larrégaray, L. Bonnet, and J. C. Rayez, Phys. Chem. Chem. Phys. (in press) **110,** 870 (1999).
[232] M. A. Bajeh, E. M. Goldfield, A. Hant, C. Kappel, A. J. H. M. Meijer, H.-R. Volpp, and J. Wolfrum, J. Phys. Chem. A **105,** 3359 (2001).
[233] H.-G. Rubahn, W. J. van der Zande, R. Zhang, M. J. Bronikowski, and R. N. Zare, Chem. Phys. Lett. **186,** 154 (1991).
[234] K. Kessler and K. Kleinermanns, J. Chem. Phys. **97,** 374 (1992).
[235] S. Seeger, V. Sick, H.-R. Volpp, and J. Wolfrum, Isr. J. Chem. **34,** 5 (1994).